# *Stable-isotope geochemistry of syntectonic veins in Paleozoic carbonate rocks in the Livingstone Range anticlinorium and their significance to the thermal and fluid evolution of the southern Canadian foreland thrust and fold belt*

**Michael A. Cooley, Raymond A. Price, T. Kurtis Kyser, and John M. Dixon**

## ABSTRACT

The Livingstone Range anticlinorium (LRA) marks a major hanging-wall ramp where the Livingstone thrust cuts approximately 1000 m (~3281 ft) between regional decollement in the upper part of the Devonian Palliser Formation and the Jurassic Fernie Formation.

Prethrusting and folding jasper ± fluorite ± sphalerite veins with halos of altered dolomitic host rock with high $^{87}Sr/^{86}Sr$ ratios (0.7094–0.7101) relative to most Paleozoic carbonate rocks (0.7081–0.7091) record percolation of fluids along basement faults that may also have contributed anomalously radiogenic strontium to diagenetically altered Paleozoic carbonate rocks throughout the Western Canada sedimentary basin.

Fluid flow that occurred during thrust-propagation folding is recorded by dolomite ± calcite veins, with $\delta^{18}O$ values that are similar to those of host rocks (–7.92 to –1.08‰ Peedee belemnite). Anomalously high equilibrium temperatures (250 ± 50°C) as determined by oxygen-isotope thermometry and slightly higher $^{87}Sr/^{86}Sr$ ratios relative to adjacent host



Manuscript received September 5, 2007; provisional acceptance December 7, 2007; revised manuscript received April 6, 2010; final acceptance January 27, 2011.
DOI:10.1306/01271107098

## AUTHORS

MICHAEL A. COOLEY ~ *Queen's University, Kingston, Ontario, Canada;*
<email address removed>

Dr. Michael A. Cooley is a Ph.D. graduate (2007) from the Department of Geological Sciences and Geological Engineering, Queen's University, Kingston, Ontario, Canada. His structural geology background includes detailed mapping of complexly deformed rocks, from polydeformed metamorphic rocks to nonmetamorphosed sedimentary rocks in thrust and fold belts. He is currently a structural geology consultant for the mineral exploration industry.

RAYMOND A. PRICE ~ *Queen's University, Kingston, Ontario, Canada;*
<email address removed>

Dr. Raymond A. Price is professor emeritus at the Department of Geological Sciences and Geological Engineering, Queen's University, Kingston, Ontario, Canada. His research in structural geology and tectonics, particularly in the Canadian Cordillera, has provided new insights on the structure and tectonic evolution of the Cordilleran foreland thrust and fold belt in Canada and for other thrust belts worldwide.

T. KURTIS KYSER ~ *Queen's University, Kingston, Ontario, Canada;*
<email address removed>

Dr. T. Kurtis Kyser is a professor of isotope geochemistry and the director of the Queen's Facility for Isotope Research at the Department of Geological Sciences and Geological Engineering, Queen's University, Kingston, Ontario, Canada. His research interests include isotope geochemistry, origin and chemical evolution of the earth, evolution of fluids in basins, low-temperature geochemistry, geochronology, environmental geochemistry, and fluid-rock interactions.

JOHN M. DIXON ~ *Queen's University, Kingston, Ontario, Canada;* <email address removed>

Dr. John M. Dixon has taught structural geology at the Department of Geological Sciences and Geological Engineering, Queen's University, Kingston, Ontario, Canada. His research of thrust and fold tectonics has generally focused on analog (centrifuge) and numerical (finite element) modeling. He is currently associate vice

president academic-international at Queen's University, but continues his research while on permanent administrative leave.


## ACKNOWLEDGEMENTS

This research was supported by Natural Sciences and Engineering Research Council grants to Raymond Price, Kurt Kyser, and John Dixon. We acknowledge the financial assistance of the sponsors of the Fold Fault Research Project. Geochemical analyses were conducted under the invaluable supervision of Kerry Klassen and Don Chipley of the Queen's University Facility for Isotope Research. Field work benefited greatly from the field assistance of Greg Cameron, Scott Conley, and Kyle Larson. We are very grateful for the constructive criticisms of Margot McMechan, Tim Diggs, and Peter D. Warwick. Digital topography has been provided by AltaLIS, Ltd., and access to well logs was provided by Nexen.

The AAPG Editor thanks the following reviewers for their work on this paper: Tim Diggs and Peter D. Warwick.


## EDITOR'S NOTE

Color version of Figure 16 may be seen in the online version of this article.


rocks indicate that they formed from formation fluids and hot basement fluids in a rock-dominated system.

Calcite veins with very low $\delta^{18}O$ values (–18 to –9‰) precipitated along faults that were active while the LRA was transported eastward by underlying thrust faults, uplifted, and rapidly cooled by infiltrating meteoric water.

Thrusting created heating in the foreland basin ahead of the deformation because of the influx of thick insulating foreland basin sediments, causing thermal maturation of hydrocarbons. As thrusting deformation advanced through the rocks, infiltrating meteoric waters cooled the rocks and hydrocarbon maturation stopped. Structural traps accumulated hydrocarbons only if they were juxtaposed over both thermally favorable and hydrocarbon-favorable source rocks.


## INTRODUCTION

Within the geologic history of every deformation belt, concurrent thermal and fluid-flow histories that are integral parts of the tectonic evolution exist. Fluids transmit heat, facilitate faulting, and transport potentially economic minerals and hydrocarbons.

By studying coal rank data of Paleocene and younger foreland basin sedimentary rocks of Alberta, Hitchon (1984) recognized that a reversal in geothermal gradient patterns had occurred during thrusting and folding, which he attributed to migration of fluids in a two-part process: (1) relatively high geothermal gradients in the western foreland basin were abruptly decreased when these rocks became incorporated into the thrust and fold belt and became topographically higher, providing the hydraulic potential for deep penetration of cold meteoric water; and (2) initially lower geothermal gradients in the undeformed eastern foreland basin were abruptly increased during thrusting, which he attributed to lateral flow of warm formation fluids that had been displaced from deep beneath the deformed belt by infiltrating meteoric fluids.

The first part of the theory of Hitchon (1984) is generally well supported by studies of the thermal history and fluid flow in the southern Canadian Cordillera (Nesbitt and Muehlenbachs, 1995; Osadetz et al., 2004) and in the Idaho-Wyoming thrust belt (Burtner and Nigrini, 1994). Nesbitt and Muehlenbachs (1995) documented meteoric water isotopic signatures in what they interpreted to be primary fluid inclusions in apparently undeformed syntectonic veins across the southern Canadian Cordillera. Apatite fission-track thermochronology and vitrinite reflectance data from the foreland thrust and fold belt in

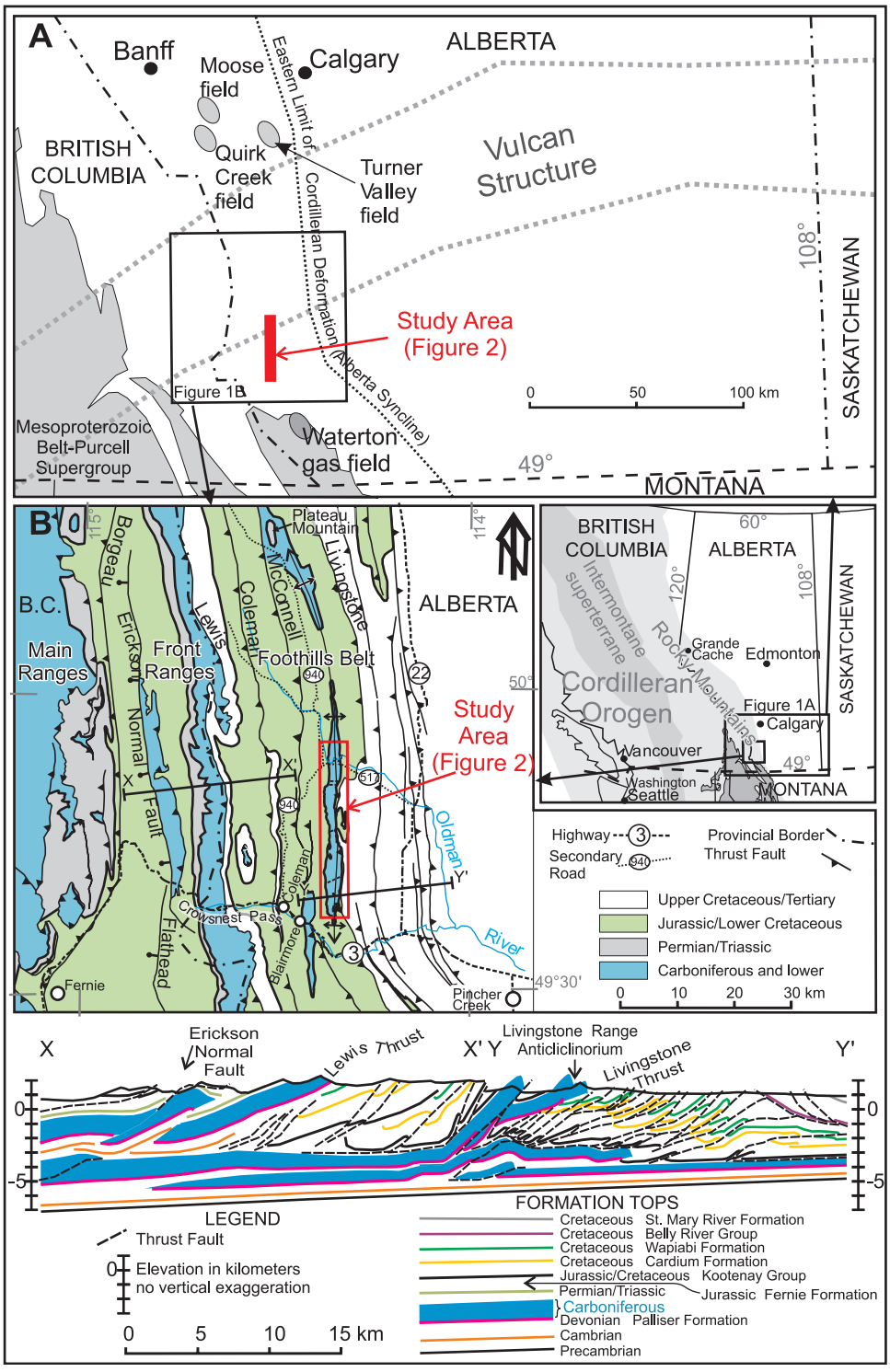


**Figure 1.** The regional geologic setting of the study area. (A) Hydrocarbon reservoir fields and geologic features described in the text. (B) The geologic map modified from Wheeler and McFeely (1991) and R. A. Price (2007, personal communication). The cross section XX′ was modified from R. A. Price (2007, personal communication). The cross section YY′ was modified from the cross section of P. MacKay (2003, personal communication).

southern Alberta and British Columbia have shown that rapid cooling of the thrust belt coincided with displacement on the Lewis thrust (Figure 1) and other related faults (Osadetz et al., 2004). A similar fluid-flow model was proposed for the Idaho-Wyoming thrust belt by Burtner and Nigrini (1994), who interpreted an eastward younging pattern of apatite fission-track cooling dates to represent the progressive eastward cooling of strata by infiltrating meteoric water as they became incorporated into

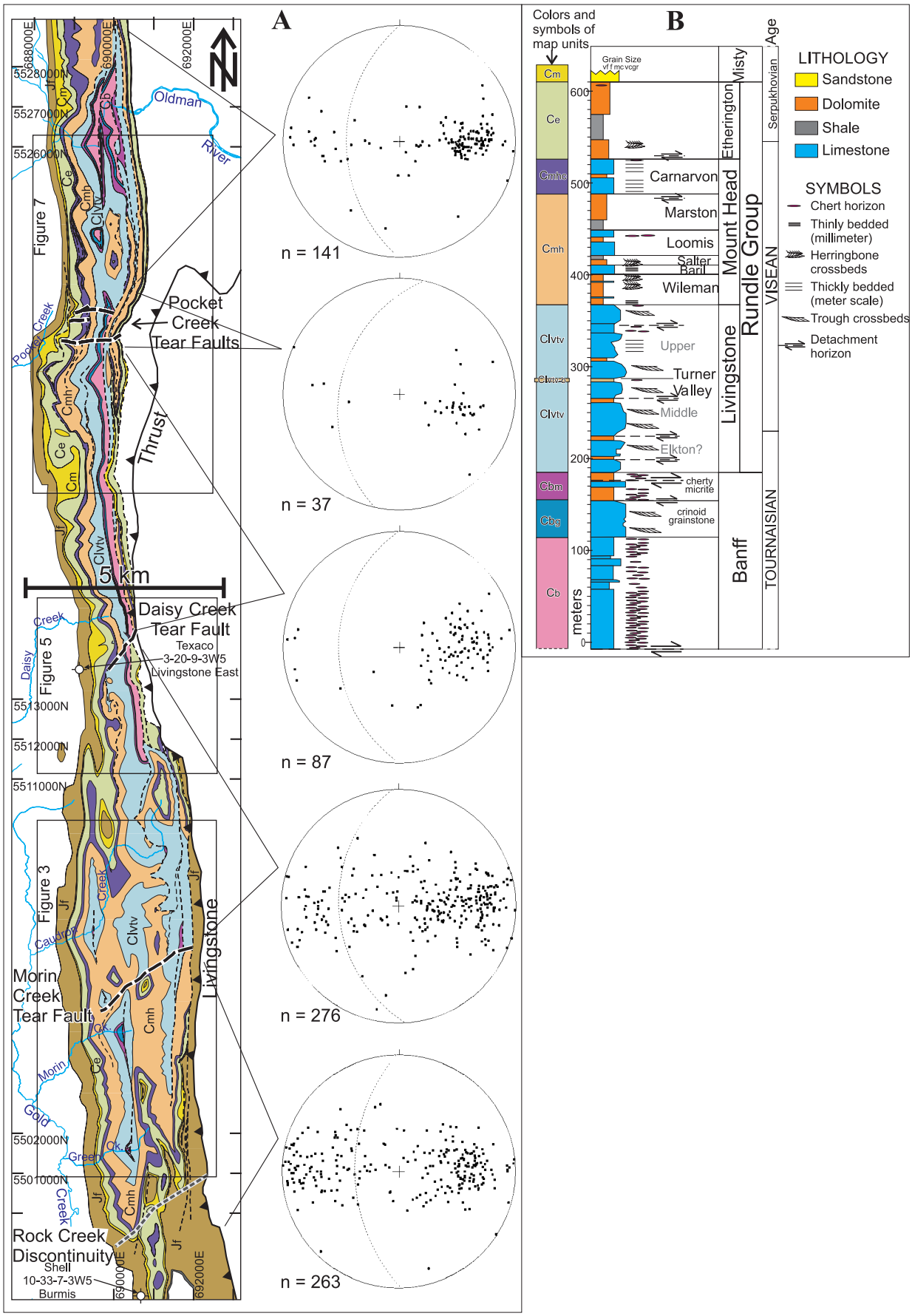
A
B
Colors and symbols of map units
Grain Size
vf f mc vcgr
Age
Serpukhovian
VISEAN
TOURNAISIAN
Misty
Etherington
Mount Head
Rundle Group
Livingstone
Banff
Carnarvon
Marston
Loomis
Salter
Baril
Wileman
Upper
Turner Valley
Middle
Elkton?
cherty micrite
crinoid grainstone
meters
600
500
400
300
200
100
0
Cm
Ce
Cmhc
Cmh
Clvtv
Cbm
Cbg
Cb
LITHOLOGY
Sandstone
Dolomite
Shale
Limestone
SYMBOLS
Chert horizon
Thinly bedded (millimeter)
Herringbone crossbeds
Thickly bedded (meter scale)
Trough crossbeds
Detachment horizon
n = 141
n = 37
n = 87
n = 276
n = 263
Pocket Creek Tear Faults
Thrust
Daisy Creek Tear Fault
Texaco 3-20-9-3W5 Livingstone East
Morin Creek Tear Fault
Rock Creek Discontinuity
Shell 10-33-7-3W5 Burmis
Figure 7
Figure 5
Figure 3
5 km
Oldman River
Pocket Creek
Daisy Creek
Morin Creek
Gold Creek
Green Creek
Cougar Creek
5528000N
5527000N
5526000N
5513000N
5512000N
5511000N
5502000N
5501000N
688000E
690000E
692000E

the thrust belt. The occurrence of veins with low $\delta^{18}O$ values along major thrust faults in the Front Ranges of the Rocky Mountains near Banff, Alberta (Kirschner and Kennedy, 2001), and in thrust-related hydrocarbon-bearing structures in the subsurface beneath the southern foothills of the Rocky Mountains (Figure 1A), including Moose field (Cioppa et al., 2000), Quirk Creek field (Al-Aasm and Lu, 1994), and Waterton gas field (Lewchuk et al., 1998), may be the isotopic record of meteoric fluid infiltration. However, the restricted presence of veins with low $\delta^{18}O$ values to within 1 m (3.3 ft) of thrusts and the absence of host rock alteration led Kirschner and Kennedy (2001) to interpret that only small amounts of meteoric fluids flowed along thrust faults in the Front Ranges of the Canadian Rocky Mountain. A major contradiction therefore exists; if meteoric waters were circulating through the thrust and fold belt in sufficient quantities to remove heat from the rock mass, then the wall rocks should exhibit significant alteration. Where is this alteration and what were the major conduits for circulation of meteoric fluids?

The heating event that occurred in the foreland basin, which Hitchon (1984) attributed to hot formation fluids that were displaced from deep beneath the deformation belt, is also recorded by a Late Cretaceous prethrusting and folding chemical remanent remagnetization event in the Rocky Mountains and Foothills of southern Alberta and British Columbia (Lewchuk et al., 1998; Cioppa et al., 2000; Enkin et al., 2000). Cioppa et al. (2000) document an increase in magnetic mineral grain size that correlates with recrystallization of microdolomite to mesodolomite, indicating that the Cretaceous chemical remagnetization is caused by recrystallization of in-situ magnetic minerals, a process that could occur simply from increased temperatures from sedimentary burial. In addition, comparison of conodont alteration index data with laboratory unblocking temperatures from paleomagnetic studies in the Western Canada sedimentary basin has led Symons and Cioppa (2002) to suggest that the widespread Cretaceous remagnetization recorded in the strata is likely caused by the thermal effects of burial and not to orogenic fluid flow. Furthermore, present-day formation fluid salinity data and geothermal data from wells in the sedimentary basin that underlies most of Alberta imply that the movement of fluids through the undeformed strata of the Alberta Basin is too slow to be capable of transporting heat by displacing formation fluids (Bachu, 1995). Although minor amounts of hot fluids may have entered the undeformed foreland basin before thrusting (Machel and Cavell, 1999) and during early stages of thrusting (Bradbury and Woodwell, 1987), no isotopic or other chemical evidence of alteration has been found in the host rocks that would document advective heating before or during thrusting deformation, as proposed by Hitchon (1984).

A principal objective of this research was to investigate the stable-isotope geochemistry of host rocks and syntectonic veins in the Livingstone Range anticlinorium (LRA) and deduce the isotopic composition of evolving formation waters that were in equilibrium with host rocks or with vein minerals throughout the geologic history. Within the LRA, deformation associated with the formation of many carbonate and quartz veins can be linked unequivocally to displacements on specific thrust faults, tear faults, and minor faults. Crosscutting relationships observed between many vein sets provide relative age constraints between different deformation events and fluid flow. This study combines fluid source information derived from their inferred isotopic compositions, oxygen-isotope thermometry of veins, and paleothermal data from coal to establish a thermal, fluid, and tectonic history for the LRA, which can be directly correlated with the thermal, fluid, and tectonic evolution—and hydrocarbon potential—of the southern Canadian foreland thrust and fold belt.

**Figure 2.** Geologic map (A) and stratigraphy (B) of the study area. The Livingstone Range anticlinorium is composed of five straight segments that are separated by regularly spaced cross-strike discontinuities. Thin dashed lines are thrust faults. Thick dashed lines are tear faults. The location of this map is shown in Figure 1. Bedding orientations within each of the five segments are shown in stereographic projections from the lower hemisphere and plotted using GEOrient 9.1 (Holcombe).

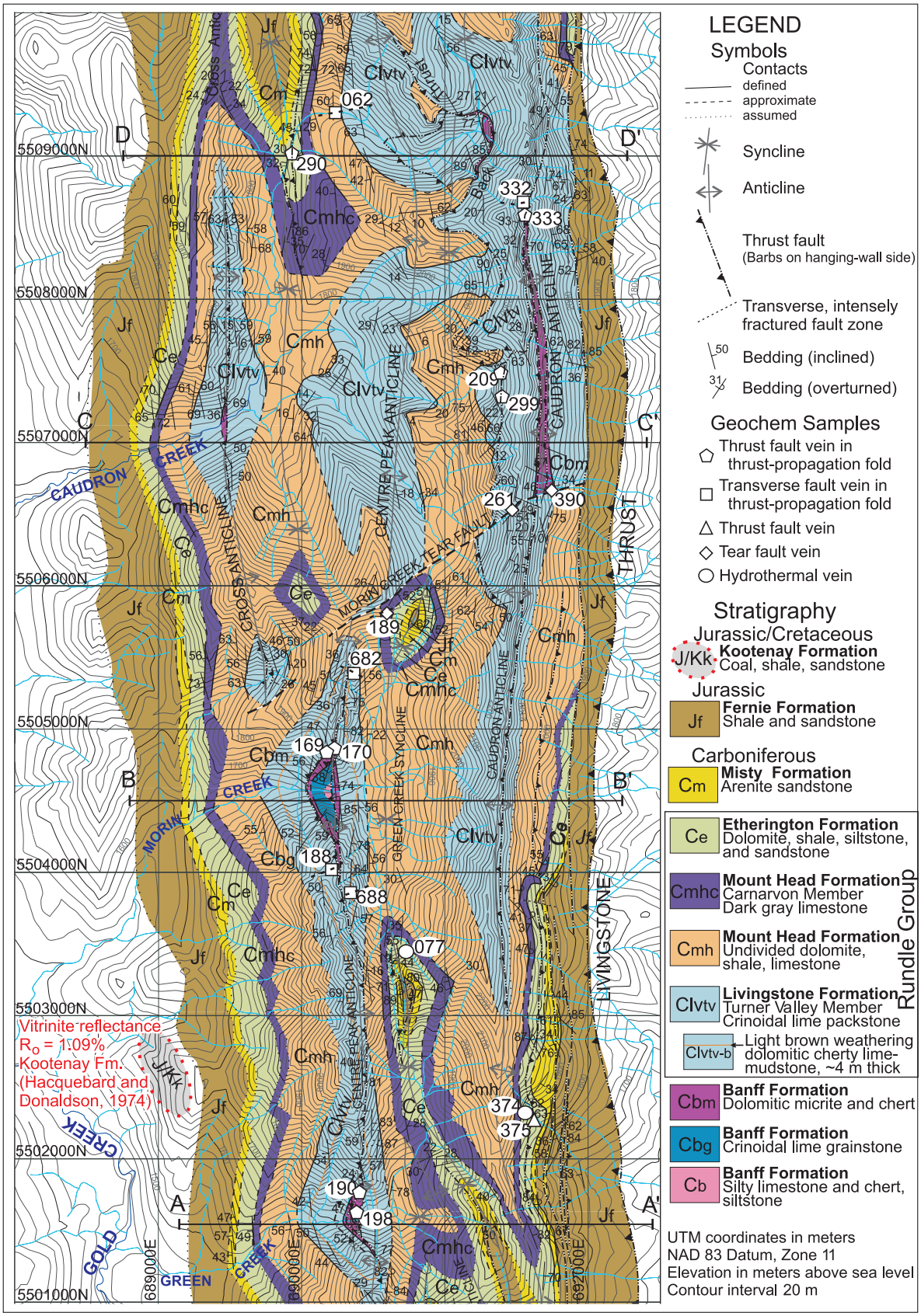


**Figure 3.** The geologic map of the southern half of the Livingstone Range anticlinorium study area. The sample localities for geochemical analysis are labeled on the map and discussed in the text.

## GEOLOGIC SETTING

The Rocky Mountains and Foothills belt of southwestern Alberta form the eastern margin of the Cordilleran foreland thrust and fold belt. The thrust and fold belt is a northeast-tapering accretionary wedge comprising sedimentary strata that have been scraped off the underriding Laurentia craton and transported eastward with the overriding Intermontane superterrane, a tectonic collage of oceanic magmatic arc and volcanic and sedimentary rocks that were obducted over and accreted to the western margin of Laurentia during the Late Jurassic to the Paleocene convergence between Laurentia and subduction zones along its western margin (Monger and Price, 1979; Price, 1981, 1994).

The structure of the accretionary wedge is dominated by east-verging listric thrust faults that flatten with depth and merge into a basal decollement that lies just above the contact between the sedimentary cover and underlying Paleoproterozoic basement. Thrust-propagation folds and fault-bend folds developed during the thrusting. The displaced and deformed rocks include the Belt-Purcell strata, which accumulated in a Mesoproterozoic intracontinental rift; the Neoproterozoic to Jurassic Cordilleran miogeocline, which accumulated along the western rifted continental margin of Laurentia; the platform cover on Laurentia, which is the lateral equivalent of the miogeocline; and the Jurassic to Eocene synorogenic foreland basin deposits that accumulated in front of the advancing accretionary wedge and were partly incorporated in it. In the Front Ranges, imbricate sheets of cratonic platform carbonate strata form conspicuous linear mountain ranges. In the Foothills, thinner imbricate slices of foreland basin siliciclastic strata form more subdued topography, but with isolated linear mountain ranges underlain by local culminations that expose Paleozoic rocks.

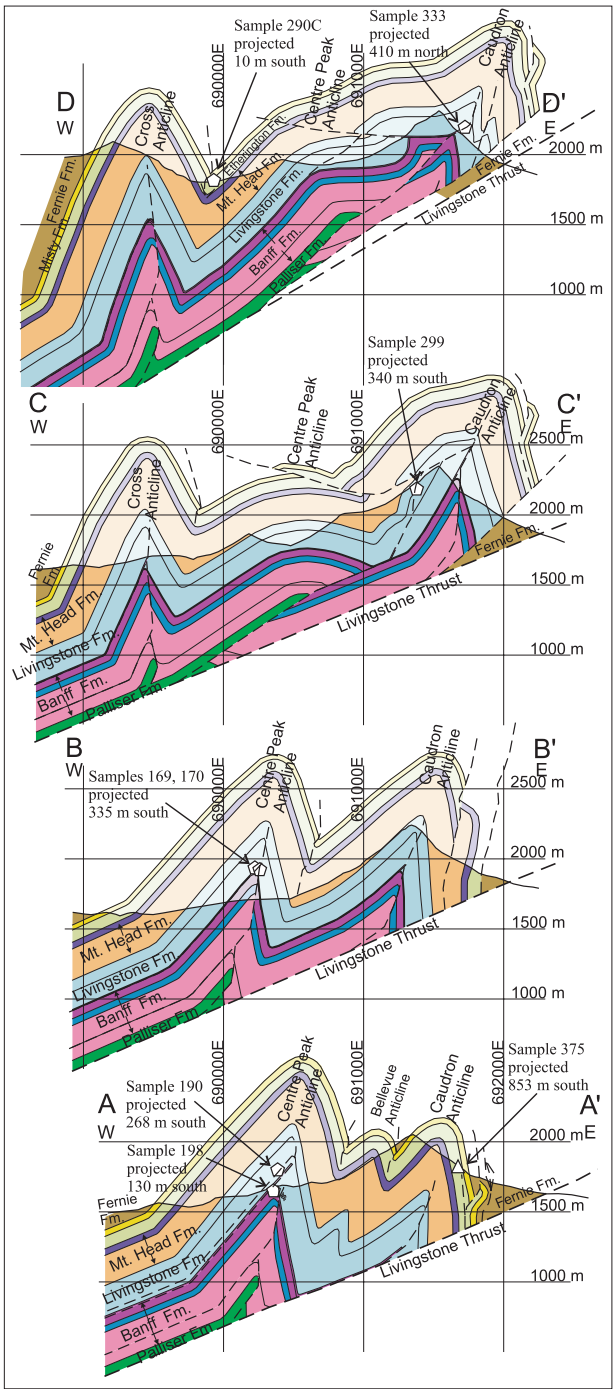


**Figure 4.** The geologic cross sections through the southern half of the Livingstone Range anticlinorium study area. The Morin Creek tear fault lies between cross sections BB′ and CC′. The locations of cross sections and symbols for geochemical samples are displayed in Figure 3.

## STRUCTURAL GEOLOGY OF THE SOUTHERN LIVINGSTONE RANGE

The following section briefly describes the structural geology of the LRA. A more complete description is presented within a separate article within this journal issue (Cooley et al., 2011) and in Cooley (2007).

The LRA is a long (65 km [40 mi]) narrow (<5 km [<3 mi] wide) north-trending horizontally

**Figure 5.** The geologic map of the Daisy Creek area. The legend for this map is the same as in Figure 3. The sample localities for geochemical analysis are labeled on the map and discussed in the text. Jf = Fernie Formation; Cm = Misty Formation; Ce = Etherington Formation; Cmhc = Carnarvon Member of the Mount Head Formation; Cmh = undivided Mount Head Formation; Clvtv = Turner Valley Member of the Livingstone Formation; Cbm = Banff Formation micrite unit; Cbg = Banff Formation grainstone unit; Cb = undivided Banff Formation.

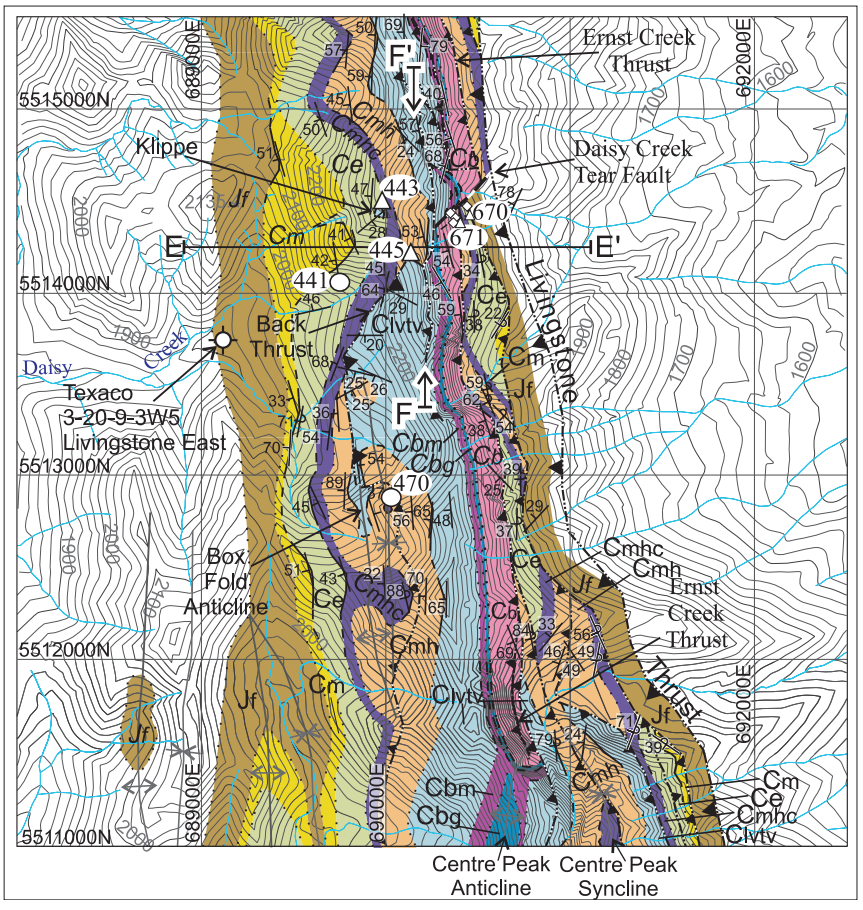


**Figure 6.** Cross section EE′ and profile section FF′ through the Daisy Creek fault system. The profile section FF′ is a view down to the west at a plane that strikes north and dips 45° eastward. The locations of the sections are shown in Figure 5. Sample localities for geochemical analysis are labeled on profile section FF′. The detailed inset in FF′ shows the structural locations of individual samples from sites 670 and 671.

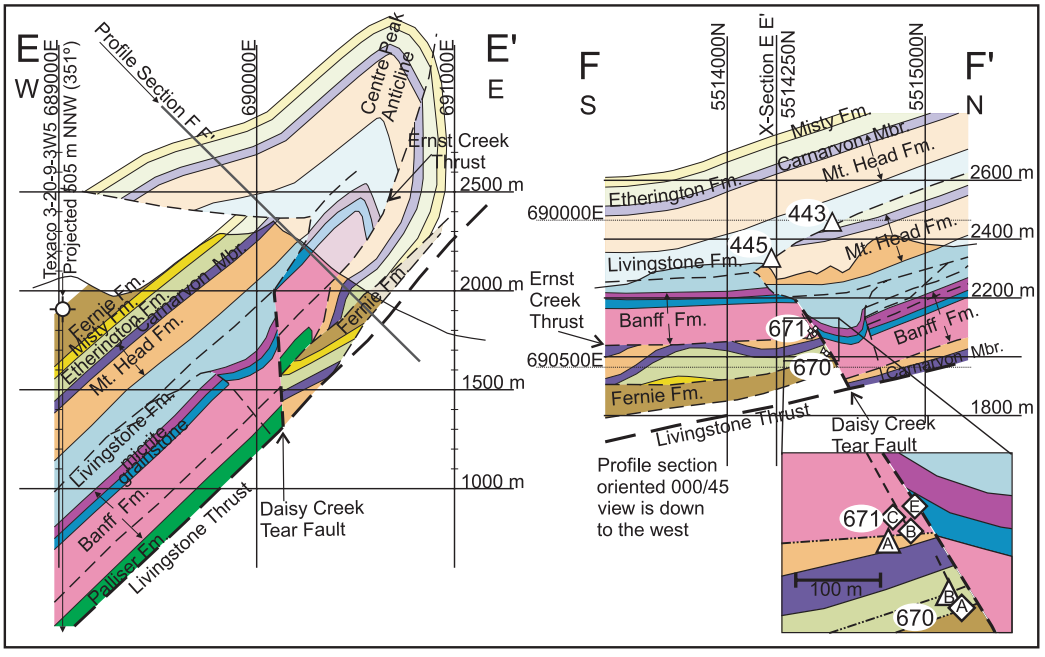

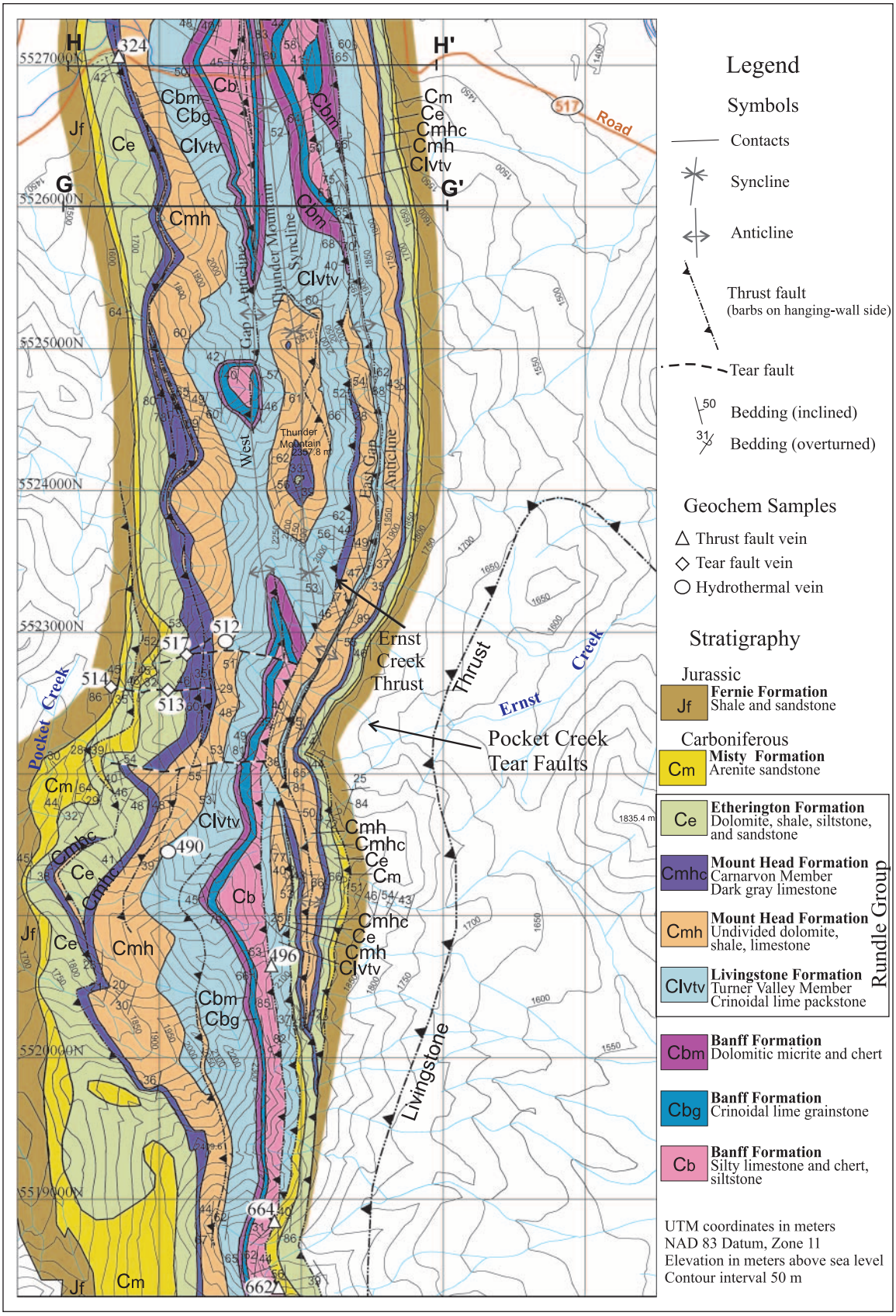


**Figure 7.** The geologic map of the northern part of the study area. Three east-west tear faults are associated with a dextral deflection of the Livingstone Range anticlinorium at Pocket Creek. The sample localities for geochemical analysis are labeled on the map and discussed in the text.

plunging structural culmination of Mississippian platformal carbonate rock that stands above the surrounding deformed foreland basin strata of the Foothills belt (Figure 1B). The LRA coincides with a major hanging-wall ramp across which the Livingstone thrust cuts approximately 1000 m (~3281 ft) upsection from a regional decollement in lime mudstones of the upper part of the Devonian Palliser Formation to another regional decollement within marine shale of the Jurassic Fernie Formation. In the southern Livingstone Range, the matching footwall ramp is located more than 30 km (>19 mi) to the west, under the Lewis thrust sheet (Price, 1981, 1994). The structure of the southern part of the LRA changes along strike as individual anticlines emerge, increase in size, and die out (Figure 2A). The changes are generally gradual, but locally, they occur abruptly across cross-strike discontinuities that coincide with lateral thrust ramps or northeast-trending "tear faults" that are kinematically linked to slip on the underlying Livingstone thrust. The Morin Creek tear fault (Figures 2A, 3, 4) and the Daisy Creek tear fault (Figures 2A, 5, 6) are interpreted to be preexisting steeply dipping east-northeast–trending faults that became reactivated as strike-slip faults during thrusting and folding. The Rock Creek discontinuity (Figure 2A) is probably the same type of reactivated fault structure, but at its present level of erosion, the only evidence for the underlying tear fault are abrupt changes in plunges of folds in the overlying Mount Head Formation and younger strata. The Pocket Creek tear faults (Figures 2A, 7) clearly differ fundamentally from the other three cross-strike discontinuities because they are east-west striking and formed within a conspicuous transverse east-west–trending dextral monoclinal flexure that has been superimposed on the entire LRA by underlying younger thrust-related structures.

The LRA is an array of linked, en-echelon, mainly chevron-style thrust-propagation folds involving the Devonian–Mississippian platformal carbonate rocks (Figure 2B) and overlying Mesozoic siliciclastic foreland basin deposits. The development of the LRA was dominated by flexural-slip thrust-propagation folding that occurred as the Livingstone thrust was propagating up the ramp through

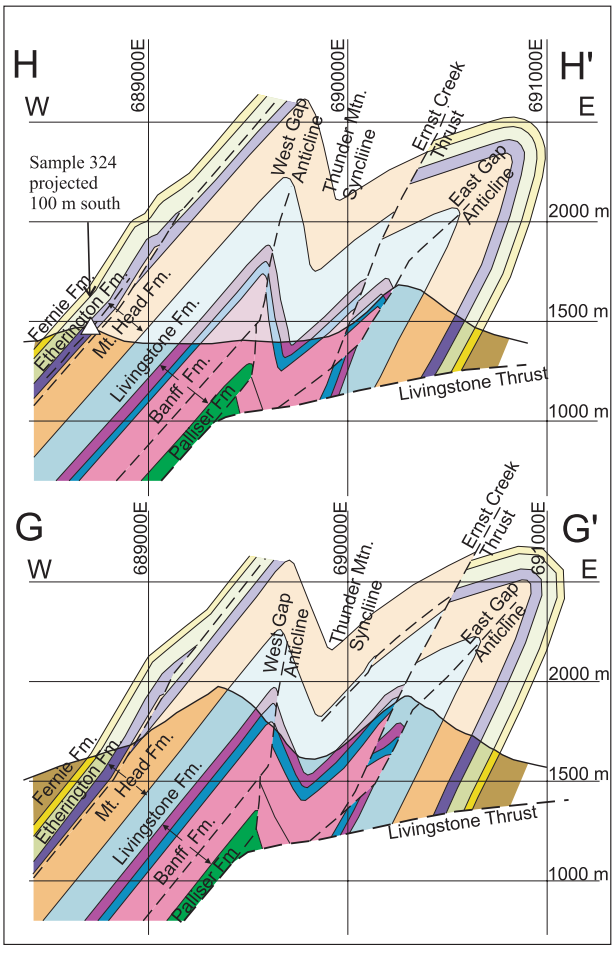


**Figure 8.** Cross sections GG′ and HH′. The locations of the sections are shown in Figure 7. Sample 324 is from a minor thrust fault that cuts the Carnarvon Member of the Mount Head Formation.

approximately 1000 m (~3281 ft) of Mississippian strata during the latest Cretaceous, and the folds are interpreted to have been fully formed by the time the Livingstone thrust began propagating along the upper detachment in the Jurassic Fernie Formation and began transporting the LRA eastward. Each chevron-style anticline is associated with one or more foreland-verging thrust faults that die out upward into the hinge zone. These blind thrusts separate steeply dipping planar east-facing forelimbs from less steeply dipping west-facing planar backlimbs (Figures 3, 4, 7–9). Above the tip lines of the blind thrust faults, the strata in the cores of the anticlines outline concentric parallel folds.

During the formation of the LRA, the Mississippian carbonate rocks underwent brittle deformation

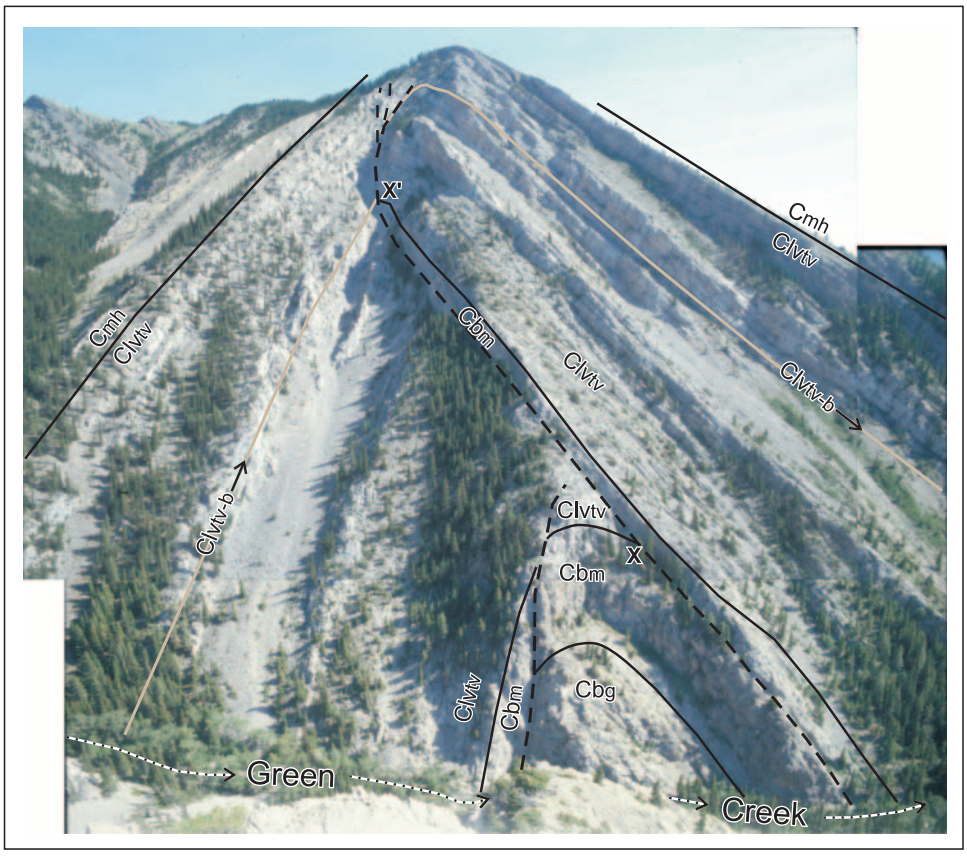


**Figure 9.** View south at the core of the Centre Peak anticline, a typical chevron-style thrust-propagation fold in the Livingstone Range anticlinorium. The thin solid lines represent stratigraphic contacts. Stratigraphic units (Cbg, Cbm, Clvtv, Clvtv-b, and Cmh) are described in the legend in Figure 3. The x and x' mark the top of the Banff Formation that has been offset by approximately 250 m (~820 ft) by a thrust fault that propagated out of the backlimb of the fold. Thrust faults are represented by thick dashed lines. Cmh = undivided Mount Head Formation; Clvtv = Turner Valley Member of the Livingstone Formation; Clvtv = Brown marker unit within the Turner Valley Member of the Livingstone Formation; Cbm = Banff Formation micrite unit; Cbg = Banff Formation grainstone unit.

that was conspicuously discontinuous and inhomogeneous at the scale of an individual outcrop (Price, 1967). The deformation involved small displacements along and across a complex array of small contraction and extension faults, interbed shear zones, and joints. These brittle fractures bounded individual blocks of rock that underwent large translation and rotation with little or no internal deformation. Substantial dilation occurred during the deformation. Stylolites record pressure solution along some fractures. Precipitation of calcite, dolomite, and quartz in dilatant fracture zones was a widespread but minor component of the deformation. These vein minerals provide the basis for investigating the geochemistry and geothermometry of pore fluids during deformation.

Regularly spaced (~150 m [~492 ft]), east-west–striking, steeply dipping zones of intense fracturing and minor faulting transect the north-south–striking limbs and hinge zones of chevron-style folds in the vicinity of Green Creek, Morin Creek, and Caudron Creek (Figure 10). The fracture zones, which commonly contain one or more discrete but discontinuous fault surfaces are commonly marked by gullies that form conspicuous erosion features in the steeper slopes and cliffs (Figure 10A, B). Offsets are commonly 1 m or less (≤3.3 ft), and the sense of displacement varies from one fault to the next. Slickenlines and slickenfibers are rare and, where preserved, are generally parallel with the bedding. Solid black hydrocarbon residues are common on fault surfaces and in fractures (Figure 10D). Rare crosscutting calcite and/or dolomite and/or hydrocarbon veins provide evidence of intermittent reactivation of the transverse fracture zones. These fractured zones appear to have developed during flexural-slip folding by reactivation of a set of preexisting steeply dipping, east-west–trending megajoints that had developed preferentially within the Livingstone Formation. These fractured zones may have been important conduits for fluid migration before, during, and after thrusting and folding; moreover, they provide a good example of the types of small-scale structures that may be important for hydrocarbon migration and accumulation.

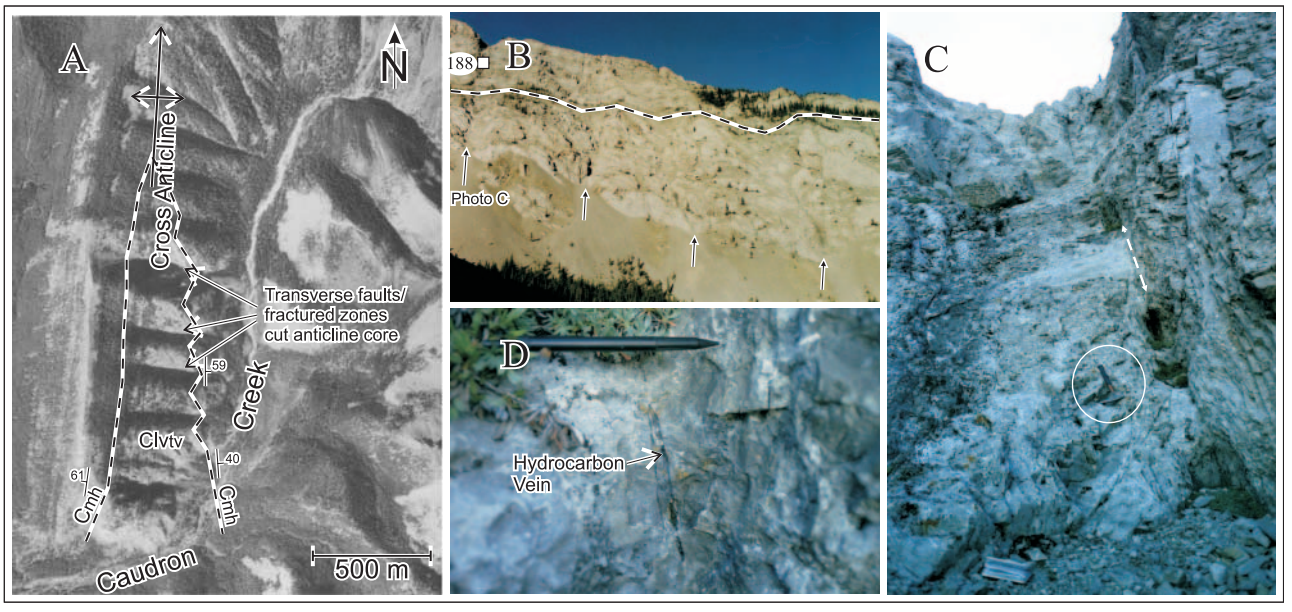


**Figure 10.** Photographs of transverse faults in the Livingstone Range anticlinorium. (A) Vertical air photograph of the cross anticline at Caudron Creek. The east-west–trending gullies mark the locations of transverse fractured zones that cut through the Turner Valley Member limestone at regularly spaced intervals in the anticlinal core. Note that most gullies do not extend into the overlying Mount Head Formation. (B) View westward at the east limb of the Centre Peak anticline south of Morin Creek. The black arrows mark the locations of transverse faults that cut through the east limb. The dashed line marks the surface trace of the hinge of the anticline core. Calcite + dolomite veins occur along a transverse fault zone at sample location 188. (C) View westward at intensely fractured limestone within a transverse fault zone visible in Figure 10B. Dashed white line with arrows points along the main fault contact. The circle at lower center of photograph outlines a 33-cm (13-in.)-long hammer for scale. (D) View to the west at a vertical transverse fault surface at lower center of photograph containing black hydrocarbon residue, a common feature of fault zones. Pencil for scale is 14 cm (5.5 in.) long.

## Descriptions of Veins

### Prethrusting Hydrothermal Veins

Deformed hydrothermal veins comprising quartz ± dolomite ± fluorite occur locally within the LRA (Figures 3–8). All of these veins are fractured, some are cut by stylolites and by younger calcite veins, consistent with having been affected by thrusting and folding deformation. Narrow alteration halos adjacent to the veins are rare. They comprise decimeter-wide zones of lighter colored dolomitic host rock (Figure 11A), which is locally silicified. Vein quartz is generally cherty with some banded jasperoid layers that locally replace host rocks (inset photo in Figure 11A). Jasperoid chert locally occurs as nodules comprising concentric layers of red chert and clear fluorite (Figure 11B, inset photo). In some thin sections, jasperoid chert contains euhedral dolomite rhombs (Figure 11C). Euhedral to subhedral rhombs of pale purple fluorite are common within late calcite along the margins of remanents of dolomitized host rock. Bedding-parallel hydrothermal veins are common within a red shale unit within the lower part of the Etherington Formation (samples 077 and 374, Figure 3; sample 441, Figure 5). Bedding-parallel veins are also present in one outcrop of Carnarvon Member of the Mount Head Formation (sample 470, Figures 5, 11C). Bedding-perpendicular veins are generally less than 3 cm (<1.2 in.) thick and less than 1 m (<3.3 ft) long. Bedding-perpendicular veins generally strike east-southeast or north-northwest when local bedding orientations are restored to horizontal. At sample location 490 (Figures 7, 11D), three parallel hydrothermal veins, which strike 101°, lie en-echelon and are right stepping along a zone that trends 110°, which implies a sinistral sense of shear. Traces of sphalerite were also found in the hydrothermal veins at sample location 490 (Figure 7).

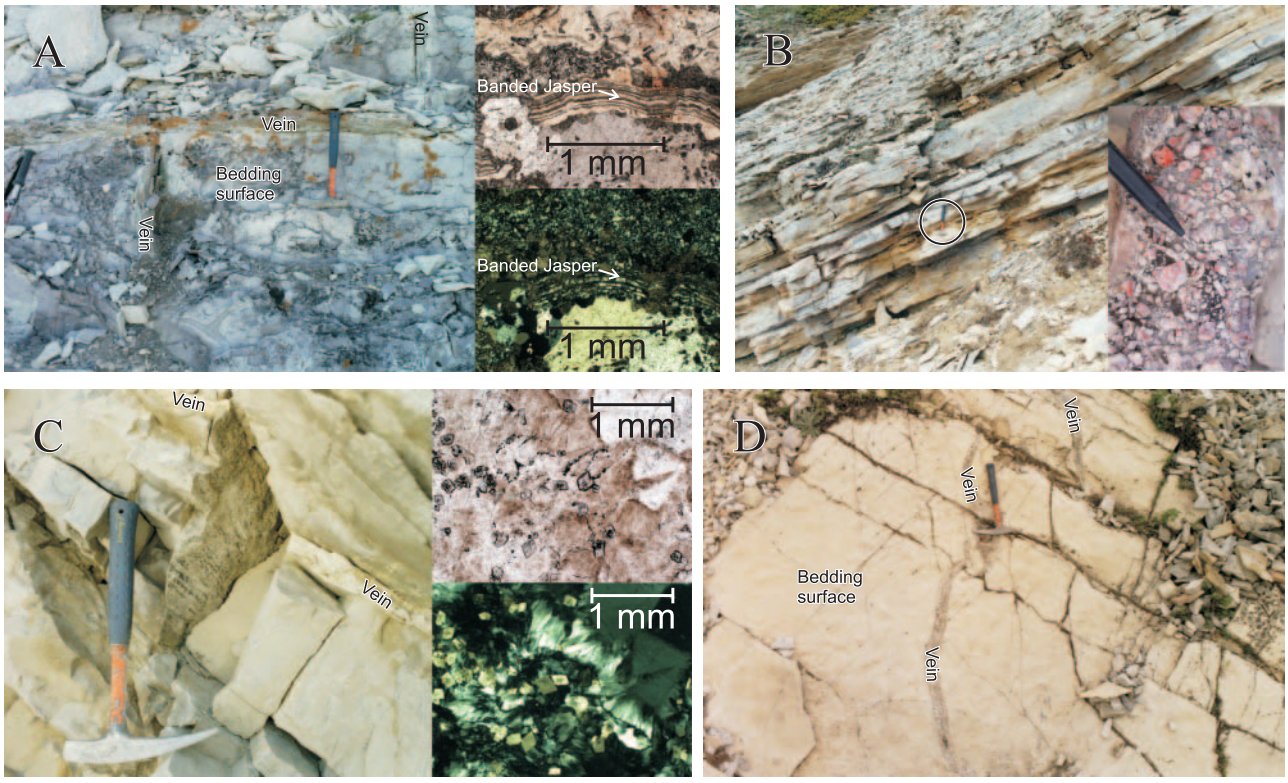


**Figure 11.** Photographs of hydrothermal veins that predate thrusting and folding. (A) The flat surface facing the field of view is an east-dipping bedding surface cut by orthogonal hydrothermal veins with narrow alteration halos in surrounding siltstone (sample locality 374, Figure 3). Inset microphotographs in (A) show thinly banded jasperoid chert cut by younger calcite veins. (B) View northward at west-dipping Etherington Formation. The hammer lies on an irregular bedding surface along which brecciated hydrothermal vein fragments are cemented by calcite as shown in detail in the inset photograph in the lower right corner (sample locality 441, Figure 5). (C) View southward at a west-dipping bedding-parallel hydrothermal vein cut by a near-vertical stylolitic surface. Inset microphotographs show euhedral dolomite crystals included in jasperoid chert (sample locality 470, Figure 5). (D) View eastward at a west-dipping bedding surface of dolomitic mudstone near the top of the Livingstone Formation. Three steeply dipping, en-echelon hydrothermal veins lie along an east-southeast–trending sinistral-sense shear zone (sample locality 490, Figure 7).

### Veins in Fault Zones

Veins occur but are rarely observed in fault zones in the study area. The veins are commonly less than 2 mm wide and less than 30 cm (<12 in.) long. Vein and host rock samples for isotopic analysis were collected from outcrops where the veins were clearly kinematically related to specific fault zones. The types of veins collected include encrustations on fault surfaces that exhibit shear steps and slickenfibers or slickenlines (Figure 12A), layered veins that record several periods of dilation and vein growth on fault surfaces (Figure 12B), sigmoidal en-echelon tension gashes that are kinematically related to movement on adjacent faults (Figure 12C), crosscutting veins that occur in intensely fractured and tightly folded hinge zones of thrust-related folds (Figure 12D, E), and breccias comprising clasts of host rock cemented by vein minerals that are present in dilatant zones along faults (Figure 12F). Brecciation was observed within a few transverse faults and tear faults, but not along thrust faults.

Veins that occur within fractured host rocks within thrust fault zones generally consist of at least two sets. The earlier vein set commonly occurs as subhorizontal to irregular networks of thin (<1 mm wide) veinlets of dark gray to black calcite ± dolomite that contain abundant intercrystalline black hydrocarbon residues. These veins fill fractures that formed during an earlier episode of locally intense brittle deformation along the fault zone. These are commonly cut by younger white to light gray calcite ± dolomite veins that are steeply

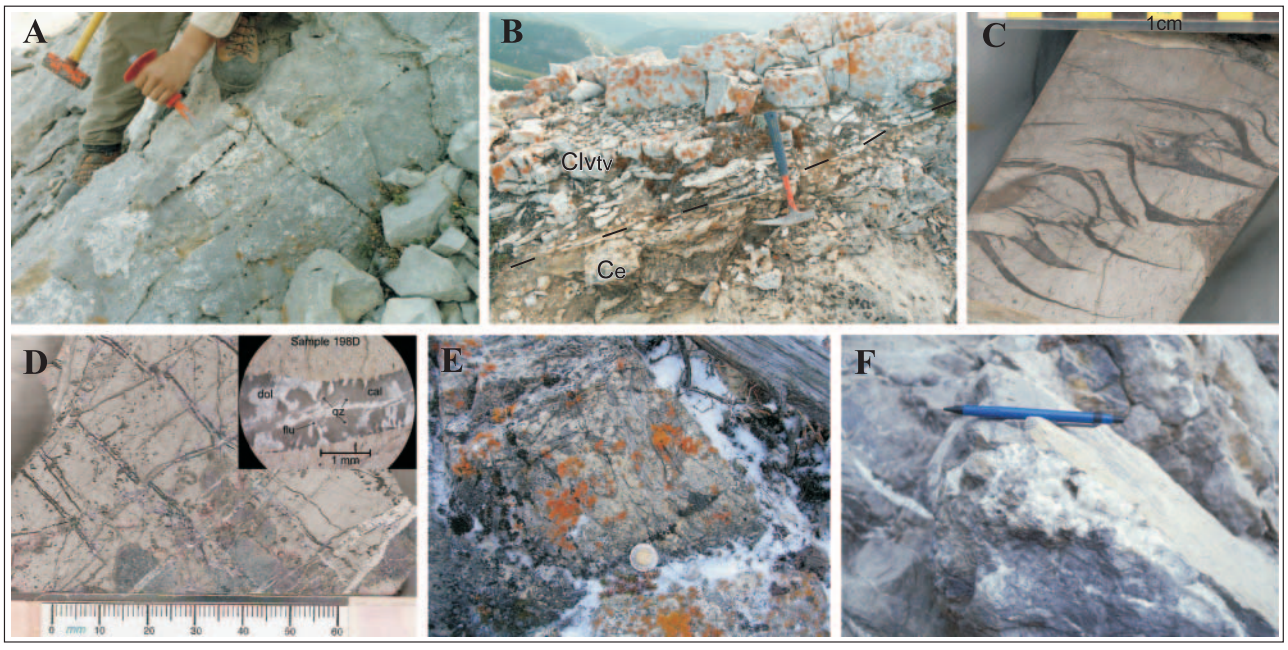


**Figure 12.** Veins associated with fault zones in the Livingstone Range anticlinorium. (A) View northward at the footwall of the Daisy Creek back thrust. Downdip-trending slickenlines are defined by white calcite encrusting the fault surface (sample location 445, Figure 5). (B) View westward at calcite veins (black dashed line) that lie along the surface of the Daisy Creek back thrust, where the Turner Valley Member of the Livingstone Formation (Clvtv) has been thrust over the Ethernington Formation (Ce) (sample location 443, Figure 5). (C) View northward at an oriented sample of micritic limestone of the Lower Turner Valley showing thrust-sense sigmoidal en-echelon calcite veins that developed in a duplex structure in the core of the Centre Peak anticline at Morin Creek (sample location 169, Figure 3). (D) Polished slab of dolomitic limestone and chert of the micrite unit of the top of the Banff Formation cut by two generations of calcite veins. The inset photograph in (D) is a close-up view of the younger vein set that contains dolomite, calcite, and quartz (sample location 198, Figure 3). (E) View westward at the outcrop where the sample in photograph (D) was taken. This fractured rock occurs within a duplex structure in the core of the Centre Peak anticline at Green Creek. (F) View southward at a transverse fault zone marked by breccia and massive white calcite veining that cuts through Upper Mount Head Formation in Caudron Creek (sample location 062, Figure 3).

dipping, thick (1–13 mm wide), few in number, and widely spaced (centimeter to decimeter spacing). These younger veins commonly contain minor traces of hydrocarbon residue. Syntectonic vein quartz is very rare but, where present, it generally occurs within faults that cut silica-rich host rocks, such as chert-bearing carbonate rocks or sandstone.

## ISOTOPE GEOCHEMISTRY

### Analytical Methods

Calcite, dolomite, and quartz in veins and in host rocks were readily identified in hand specimens by etching surfaces with 10% HCl. Calcite readily dissolves to form vitreous dull gray recessive areas, whereas white dolomite crystals and colorless euhedral quartz crystals stand out in relief. Mineral growth textures were also examined in thin sections with a petrographic microscope and with cathodoluminescence to confirm that no apparent zonation patterns exist within individual crystals or within the veins.

Powdered samples of calcite and dolomite were collected from individual veins and from host rocks using a dental drill with an approximate diameter of 0.33 mm. Quartz was collected from one vein by dissolving the calcite and dolomite in HCl and handpicking residual quartz crystals.

The $\delta^{18}O$ and $\delta^{13}C$ values for calcite or dolomite in veins and in host rocks were measured in carbon dioxide ($CO_2$) released from 5- to 10-mg powdered samples reacted with 100% phosphoric acid, following a method modified from that of

McCrea (1950). Nine samples consisting of mixtures of both calcite and dolomite were processed by differential dissolution to separate the $CO_2$ evolved from each mineral. The accuracy of this method was verified for one sample for which the calcite and dolomite were separated manually. Isotopic compositions were measured on a Finnigan Mat 252 isotope ratio mass spectrometer at the Queen's Facility for Isotope Research (Queen's University, Kingston, Ontario, Canada). An additional 99 analyses were done using a ThermoFinnigan gas bench continuous flow apparatus connected to a Thermo-Finnigan Delta Plus XP isotope ratio mass spectrometer at the Queen's Facility for Isotope Research using helium as the carrier gas. For this procedure, 0.5 mg of pure calcite or pure dolomite was reacted with 100% anhydrous phosphoric acid at 75°C.

The $\delta^{18}O$ values of quartz samples were measured using bromine pentafluoride (Clayton and Mayeda, 1963). The $\delta^{18}O$ values were measured on a Finnigan Mat 252 isotope ratio mass spectrometer at the Queen's Facility for Isotope Research.

The $\delta^{18}O$ and $\delta^{13}C$ values for carbonates and $\delta^{18}O$ values for quartz are reported relative to Vienna Peedee belemnite using delta ($\delta$) notation in units of per mil (‰). The $\delta = ([R_{sample} - R_{standard}] - 1) \times 1000$ where $R$ represents $^{13}C/^{12}C$ or $^{18}O/^{16}O$. Replicate analyses indicate a reproducibility of ±0.2‰ for both $^{13}C/^{12}C$ and $^{18}O/^{16}O$.

Temperatures of vein formation were calculated for oxygen-bearing mineral pairs that were assumed to have precipitated together in equilibrium using the calcite-water fractionation factors of O'Neil et al. (1969), dolomite-water fractionation factors of Matthews and Katz (1977), and quartz-water fractionation factors of Clayton et al. (1972). For each mineral pair, the two corresponding fractionation factor equations were combined to cancel the water terms and solve for temperature. Temperature calculations have an associated error of approximately ±50°C. The $\delta^{18}O$ values of the water from which the mineral pairs formed can then be calculated, however, the ±50°C temperature error corresponds to a $\delta^{18}O$ error for the water of +1.7/–2.3‰ for calcite-water calculations and +1.9/–2.5‰ for dolomite-water calculations.

Sample preparation for strontium isotopic analyses involved dissolving approximately 20 mg of powdered sample in 10% HCl, centrifuging, evaporating the solute, and redissolving it in sufficient 2% nitric acid solution to bring the Sr content to a suitable concentration for analysis. Strontium isotope ratio measurements were done with a NEPTUNE HR-ICP-MS (ThermoFinnigan, Bremen, Germany) at the Queen's Facility for Isotope Research. Sample inlet is via an Elemental Scientific PFA nebulizer (100 $\mu$L/min) with a cyclonic Scott spray chamber with aluminum cones. Typical operating conditions produce a beam of approximately $7.5 \times 10^{-11}$ amperes for $^{88}Sr$ from a 300 ppb Sr solution. Typical operating parameters were RF power, 1200; guard electrode, on; cool gas, 16.00 L/m; aux gas, 1.00 L/m; and nebulizer gas, 1.00 L/m. Each sample measurement consisted of seven blocks with nine cycles per block and an integration time of 8.389 sec. Peak center was at the beginning of each sample, and the amplifiers were rotated and the baselines were measured (0.5 amu) for each block. The $^{83}Kr$ is measured to correct for Kr interference on $^{84}Sr$ and $^{86}Sr$, and the $^{85}Rb$ is measured to correct for $^{87}Rb$ interference on $^{87}Sr$. Measurements of standard reference material NIST SRM987 had a value of 0.710240, and replicate analyses indicate a precision of ±0.00010 ($2\sigma$).

## Results

Carbonate samples of 35 host rocks and 33 veins were analyzed for their oxygen and carbon isotopic compositions (Table 1; Figure 13).

## Host Rocks

The $\delta^{18}O$ values of 35 host rock samples range from –12.3 to –0.7‰ (Figure 13). Thirteen of these samples consist of diagenetic dolomite, and 19 consist of either pure calcite or the calcite component of weakly dolomitized host rock. These $\delta^{18}O$ values, which are lower than the proposed value of approximately 0‰ for Mississippian seawater carbonate (Killingly, 1983; Muehlenbachs, 1998), are similar to those determined for diagenetically altered Mississippian carbonate host rocks that occur

**Table 1.** Isotopic Compositions of Host Rocks and Veins Collected from the Livingstone Range Anticlinorium

| Sample | Mineral | East UTM | North UTM | $\delta^{13}C$ (‰)* | $\delta^{18}O$ (‰)* | $^{87}Sr/^{86}Sr$ | Structure | Host Rock |
|---|---|---|---|---|---|---|---|---|
| 062C-R | Dolomite | 690220 | 5509314 | 2.2 | −4.5 | 0.70908 | Tear fault | Cmh** |
| 062C-V1 | Calcite | 690220 | 5509314 | −3.0 | −4.4 | 0.70896 | Tear fault | |
| 062C-V2 | Calcite | 690220 | 5509314 | −1.0 | −2.4 | 0.70906 | Tear fault | |
| 077A-R | Dolomite | 690661 | 5503452 | −0.6 | −4.8 | 0.70990 | Predeformation hydrothermal alteration | Ce** lower |
| 077A-V | Calcite | 690661 | 5503452 | −6.7 | −16.9 | 0.70914 | Thrust fault | |
| 077B-R | Dolomite | 690661 | 5503452 | 1.3 | −2.1 | 0.71002 | Predeformation hydrothermal alteration | Ce** lower |
| 169A-R | Calcite | 690205 | 5504835 | 1.5 | −4.3 | | Thrust fault in thrust-propagation fold | Clvtv** lower |
| 169A-V | Calcite | 690205 | 5504835 | 0.9 | −5.4 | | Thrust fault in thrust-propagation fold | |
| 170A-R | Calcite | 690222 | 5504835 | 1.5 | −4.4 | 0.70812 | Thrust fault in thrust-propagation fold | Clvtv** lower |
| 170A-V1 | Calcite | 690222 | 5504835 | 1.4 | −4.7 | | Thrust fault in thrust-propagation fold | |
| 170A-V2 | Calcite | 690222 | 5504835 | 0.1 | −6.1 | 0.70837 | Thrust fault in thrust-propagation fold | |
| 188A-Rcal | Calcite | 690220 | 5504030 | 2.1 | −6.5 | 0.70862 | Transverse fault in thrust-propagation fold | Clvtv** lower |
| 188A-Rdol | Dolomite | 690220 | 5504030 | 3.0 | −5.9 | | Transverse fault in thrust-propagation fold | Clvtv** lower |
| 188A-V1 | Calcite | 690220 | 5504030 | 2.3 | −6.6 | | Transverse fault in thrust-propagation fold | |
| 188A-V2cal | Calcite | 690220 | 5504030 | −1.1 | −5.3 | 0.70877 | Transverse fault in thrust-propagation fold | |
| 188A-V2dol | Dolomite | 690220 | 5504030 | −0.2 | −4.3 | | Transverse fault in thrust-propagation fold | |
| 189A-R | Calcite | 690556 | 5505856 | 0.0 | −6.4 | | Tear fault Morin Creek | Cmhc** |
| 189A-V1 | Calcite | 690556 | 5505856 | −0.3 | −6.3 | | Tear fault Morin Creek | |
| 189C-R | Calcite | 690556 | 5505856 | −0.1 | −5.8 | | Tear fault Morin Creek | Cmhc** |
| 189C-V3 | Calcite | 690556 | 5505856 | −2.1 | −4.5 | | Tear fault Morin Creek | |
| 190A-R | Calcite | 690400 | 5501768 | 2.1 | −3.5 | | Thrust fault in thrust-propagation fold | Cbm** |
| 190A-V2cal | Calcite | 690400 | 5501768 | 0.7 | −6.0 | | Thrust fault in thrust-propagation fold | |
| 190A-V2dol | Dolomite | 690400 | 5501768 | 1.9 | −4.8 | | Thrust fault in thrust-propagation fold | |
| 198B-R | Calcite | 690381 | 5501617 | 1.7 | −2.8 | 0.70907 | Thrust fault in thrust-propagation fold | Cbm** |
| 198B-V1 | Calcite | 690381 | 5501617 | 1.4 | −4.7 | 0.70886 | Thrust fault in thrust-propagation fold | |
| 198B-V2cal | Calcite | 690381 | 5501617 | 0.5 | −6.2 | 0.70889 | Thrust fault in thrust-propagation fold | |
| 198B-V2dol | Dolomite | 690381 | 5501617 | 0.9 | −5.1 | 0.70889 | Thrust fault in thrust-propagation fold | |
| 198B-V2dol | Dolomite | 690381 | 5501617 | 1.0 | −5.0 | | Thrust fault in thrust-propagation fold | |
| 198D-R | Dolomite | 690381 | 5501617 | 2.3 | −2.4 | | Thrust fault in thrust-propagation fold | Cbm** |
| 198D-V1 | Calcite | 690381 | 5501617 | 1.4 | −4.7 | | Thrust fault in thrust-propagation fold | |
| 198D-V2cal | Calcite | 690381 | 5501617 | 1.3 | −5.3 | | Thrust fault in thrust-propagation fold | |
| 198D-V2dol | Dolomite | 690381 | 5501617 | 2.4 | −4.0 | | Thrust fault in thrust-propagation fold | |
| 198D-V2qz | Quartz | 690381 | 5501617 | | −3.0 | | Thrust fault in thrust-propagation fold | |
| 261-R | Calcite | 691481 | 5506537 | 2.1 | −6.7 | 0.70863 | Tear fault Morin Creek | Clvtv** middle |
| 261-V | Calcite | 691481 | 5506537 | 0.2 | −6.5 | 0.70880 | Tear fault Morin Creek | |
| 209-R (altered) | Calcite | 691359 | 5507445 | 0.51 | −12.03 | | Thrust fault in thrust-propagation fold (altered) | Clvtv** upper |
| 290C-R | Dolomite | 689925 | 5509008 | −1.2 | −2.4 | 0.70857 | Thrust fault in thrust-propagation fold | Ce** upper |
| 290C-V1cal | Calcite | 689925 | 5509008 | −2.4 | −5.7 | 0.70908 | Thrust fault in thrust-propagation fold | |
| 290C-V1dol | Dolomite | 689925 | 5509008 | −1.9 | −5.2 | | Thrust fault in thrust-propagation fold | |
| 299B-Rdol | Dolomite | 691362 | 5507340 | 2.1 | −0.7 | 0.70822 | Thrust fault in thrust-propagation fold | Clvtv** upper |
| 299B-V1 | Calcite | 691362 | 5507340 | −1.5 | −5.2 | 0.70860 | Thrust fault in thrust-propagation fold | |
| 299B-V2 | Calcite | 691362 | 5507340 | −0.7 | −4.9 | 0.70858 | Thrust fault in thrust-propagation fold | |
| 324Z-R | Calcite | 688654 | 5527100 | −0.1 | −1.7 | | Tear fault | Cmhc** |
| 324Z-V2 | Calcite | 688654 | 5527100 | −4.4 | −8.3 | | Tear fault | |
| 332B-R | Calcite | 691566 | 5508672 | 1.6 | −3.9 | 0.70846 | Transverse gault in thrust-propagation fold | Clvtv** lower |
| 332B-V2 | Calcite | 691566 | 5508672 | −0.8 | −3.5 | 0.70897 | Transverse fault in thrust-propagation fold | |

**Table 1.** Continued

| Sample | Mineral | East UTM | North UTM | $\delta^{13}C$ (‰)* | $\delta^{18}O$ (‰)* | $^{87}Sr/^{86}Sr$ | Structure | Host Rock |
|---|---|---|---|---|---|---|---|---|
| 333B-R | Calcite | 691559 | 5508590 | 2.9 | −6.1 | | Thrust fault in thrust-propagation fold | Clvtv** lower |
| 333B-V1 | Calcite | 691559 | 5508590 | 1.7 | −7.5 | | Thrust fault in thrust-propagation fold | |
| 333B-V2 | Calcite | 691559 | 5508590 | 1.8 | −7.9 | | Thrust fault in thrust-propagation fold | |
| 375A-V | Calcite | 691587 | 5502353 | −5.9 | −17.8 | 0.70848 | Thrust fault | |
| 390A-V | Calcite | 691722 | 5506652 | −0.5 | −3.7 | | Tear fault Morin Creek | |
| 390B-R | Calcite | 691722 | 5506652 | 0.9 | −6.8 | | Tear fault Morin Creek | Cbm** |
| 443-V1 | Calcite | 689967 | 5514481 | −21.6 | −16.1 | | Thrust fault | |
| 443-V2 | Calcite | 689967 | 5514481 | −19.0 | −17.1 | | Thrust fault | |
| 445C-Rdol | Dolomite | 690122 | 5514194 | 1.9 | 4.9 | | Thrust fault | Cmh** |
| 445-V1centre | Calcite | 690122 | 5514194 | −15.3 | −18.0 | 0.70845 | Thrust fault | |
| 445-V2margin | Calcite | 690122 | 5514194 | −13.8 | −17.6 | 0.70874 | Thrust fault | |
| 490A-V cal | Calcite | 689019 | 5521440 | 0.7 | −9.3 | 0.70927 | Predeformation hydrothermal alteration | |
| 490B-R dol | Dolomite | 689019 | 5521440 | 2.1 | −1.3 | 0.70937 | Predeformation hydrothermal alteration | Clvtv** upper |
| 496-R (altered) | Calcite | 689771 | 5520654 | −0.4 | −12.3 | | Thrust fault with altered host rocks | Clvtv** middle |
| 496-V | Calcite | 689771 | 5520654 | −1.3 | −5.2 | | Thrust fault | |
| 503-V | Calcite | 688740 | 5522057 | −0.47 | −9.58 | | Tear fault Pocket Creek | |
| 505-V | Calcite | 688893 | 5522057 | −5.18 | −6.56 | | Tear fault Pocket Creek | |
| 512-R | Dolomite | 689489 | 5522886 | 2.3 | −2.5 | 0.71012 | Predeformation hydrothermal alteration | Cmh** |
| 513-R | Dolomite | 689020 | 5522599 | −3.4 | −4.1 | | Tear fault Pocket Creek | Ce** middle |
| 513-V1 | Calcite | 689020 | 5522599 | −10.5 | −11.5 | | Tear fault Pocket Creek | |
| 513-V2 | Calcite | 689020 | 5522599 | −5.5 | −11.8 | | Tear fault Pocket Creek | |
| 514-R | Calcite | 688658 | 5522634 | −1.2 | −6.4 | | Tear fault Pocket Creek | Jf** |
| 514-V | Calcite | 688658 | 5522634 | −2.1 | −10.5 | | Tear fault Pocket Creek | |
| 517A-R | Calcite | 689185 | 5522850 | −2.6 | −6.3 | | Tear fault Pocket Creek | Cmhc** |
| 517A-V | Calcite | 689185 | 5522850 | −11.2 | −13.1 | | Tear fault Pocket Creek | |
| 662B-breccia | Calcite | 689839 | 5518301 | −1.3 | −6.1 | | Thrust fault | Ce** middle |
| 662B-V | Calcite | 689839 | 5518301 | −4.1 | −8.7 | | Thrust fault | |
| 662C-R | Calcite | 689839 | 5518301 | 1.2 | −5.3 | | Thrust fault | Ce** middle |
| 662C-V1 | Calcite | 689839 | 5518301 | 0.2 | −6.8 | | Thrust fault | |
| 662C-V2 | Calcite | 689839 | 5518301 | −2.6 | −12.3 | | Thrust fault | |
| 662D-R | Dolomite | 689839 | 5518301 | 2.4 | −1.1 | | Thrust fault | Cb** upper |
| 662D-V | Dolomite | 689839 | 5518301 | 1.3 | −5.1 | | Thrust fault | |
| 664A-V1 | Calcite | 689809 | 5518833 | −7.1 | −9.7 | | Thrust fault | |
| 670A-V1 | Dolomite | 690435 | 5514459 | −3.0 | 0.4 | 0.70983 | Tear fault Daisy Creek | |
| 670B-R (altered) | Calcite | 690435 | 5514459 | −2.5 | −10.8 | 0.70981 | Tear fault Daisy Creek, altered host rock | Ce** middle |
| 670B-V2 | Calcite | 690435 | 5514459 | −4.5 | −16.2 | 0.70885 | Thrust fault | |
| 670B-V3 | Calcite | 690435 | 5514459 | −12.1 | −16.5 | 0.70923 | Thrust fault | |
| 671A-R | Dolomite | 690400 | 5514442 | 0.9 | −7.4 | | Thrust fault | Cb** upper |
| 671A-V1 | Calcite | 690400 | 5514442 | 0.8 | −6.4 | | Thrust fault | |
| 671A-V2 | Calcite | 690400 | 5514442 | −3.3 | −10.7 | | Thrust fault | |
| 671B-R | Calcite | 690400 | 5514442 | 1.7 | −6.3 | | Tear fault Daisy Creek | Cb** upper |
| 671B-V | Calcite | 690400 | 5514442 | −0.2 | −7.0 | | Tear fault Daisy Creek | |
| 671C-V | Calcite | 690400 | 5514442 | −0.6 | −4.2 | | Tear fault Daisy Creek | |
| 671E-V | Calcite | 690400 | 5514442 | −2.1 | −7.1 | | Tear fault Daisy Creek | |
| 682A-R | Calcite | 690360 | 5505393 | 3.1 | −5.1 | | Thrust fault in thrust-propagation fold | Clvtv** upper |

**Table 1.** Continued

| Sample | Mineral | East UTM | North UTM | $\delta^{13}C$ (‰)* | $\delta^{18}O$ (‰)* | $^{87}Sr/^{86}Sr$ | Structure | Host Rock |
|---|---|---|---|---|---|---|---|---|
| 682A-V | Calcite | 690360 | 5505393 | 0.9 | –5.5 | | Thrust fault in thrust-propagation fold | |
| 688A-R | Calcite | 690349 | 5503866 | 2.5 | –6.7 | | Transverse fault in thrust-propagation fold | Clvtv** middle |
| 688A-V1 | Calcite | 690349 | 5503866 | 1.4 | –6.0 | | Transverse fault in thrust-propagation fold | |
| 688A-V2cal | Calcite | 690349 | 5503866 | –0.6 | –5.8 | | Transverse fault in thrust-propagation fold | |
| 688A-V2dol | Dolomite | 690349 | 5503866 | 1.8 | –4.6 | | Transverse fault in thrust-propagation fold | |

*The $\delta^{18}O$ and $\delta^{13}C$ values are reported relative to Vienna Peedee belemnite in units of per mil (‰). Host rocks are denoted by sample numbers that end with R, Rcal, or Rdol. Vein sample numbers end with V, V1, V2, and so on, where V2 indicates a younger crosscutting vein set. Three hydrothermal vein samples are mentioned in the text but were not analyzed (374, 441, 470).

**Jf = Fernie Formation; Cm = Misty Formation; Ce = Etherington Formation; Cmhc = Carnarvon Member of Mount Head Formation; Cmh = undivided Mount Head Formation; Clvtv = Turner Valley Member of the Livingstone Formation; Clvtv-b = Brown marker unit within the Turner Valley Member of the Livingstone Formation; Cbm = Banff Formation micrite unit; Cbg = Banff Formation grainstone unit; Cb = undivided Banff Formation.

along strike to the north and south in the Foothills of the Rocky Mountains (Al-Aasm and Lu, 1994; Lewchuk et al., 1998; Cioppa et al., 2000).

The $\delta^{13}C$ values of unaltered strata that are older than the Carnarvon Member of the Mount Head Formation (these include the Banff Formation, Livingstone Formation, and the lower part of the Mount Head Formation) range from +0.8 to +3.1‰ (Figure 13; Table 1). These values are similar to those determined by Veizer et al. (1999) for host rocks of equivalent age from Bochum, Germany, and Ottawa, Canada.

The $\delta^{13}C$ values of host rocks from the Carnarvon Member of the Mount Head Formation and from the overlying Etherington Formation range from –3.4 to +1.3‰ (Figure 13). This range of $\delta^{13}C$ values is at least 1.7‰ lower than the value of approximately +3.0‰ shown by data presented by Veizer et al. (1999) for seawater carbonate rocks of equivalent age.

Three host rock samples in Figure 13 have abnormally low $\delta^{18}O$ values that range from –12.3 to –10.8‰ (samples 209-R, 670B-R, and 496-R in Table 1). These three host rocks, which occur along

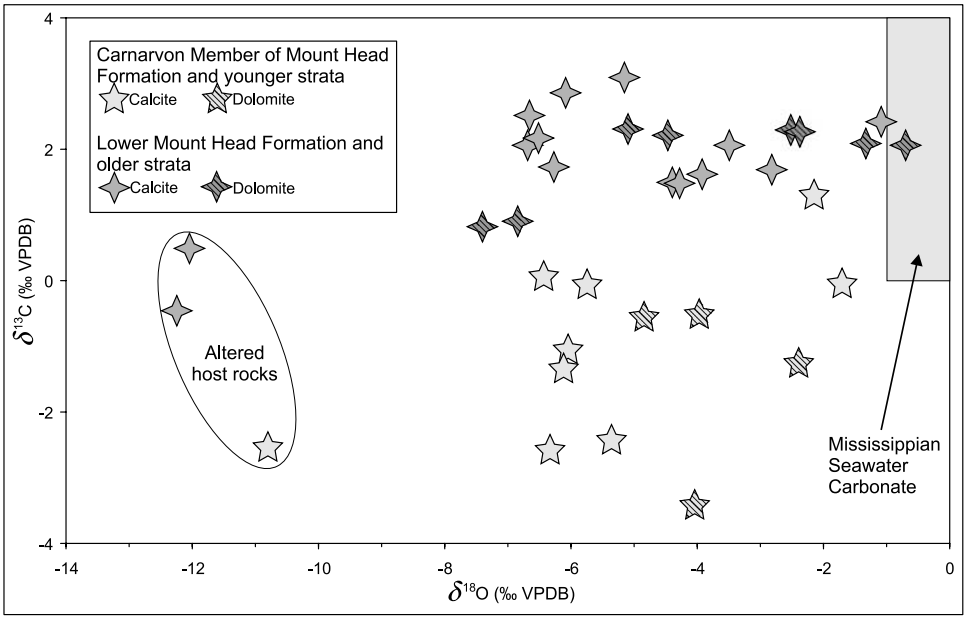


**Figure 13.** The $\delta^{18}O$ versus $\delta^{13}C$ values of host rock samples collected from the Livingstone Range anticlinorium study area. Host rocks from the Carnarvon Member of the Mount Head Formation and younger units have $\delta^{13}C$ values that are consistently lower than those of older units. Three host rock samples with $\delta^{18}O$ values less than –10‰ are from thrust fault zones where host rocks have been altered. The shaded box represents proposed Mississippian Seawater carbonate composition, where the $\delta^{18}O$ range is based on Killingly (1983) and Muehlenbachs (1998) and the $\delta^{13}C$ range is based on Veizer et al. (1999).

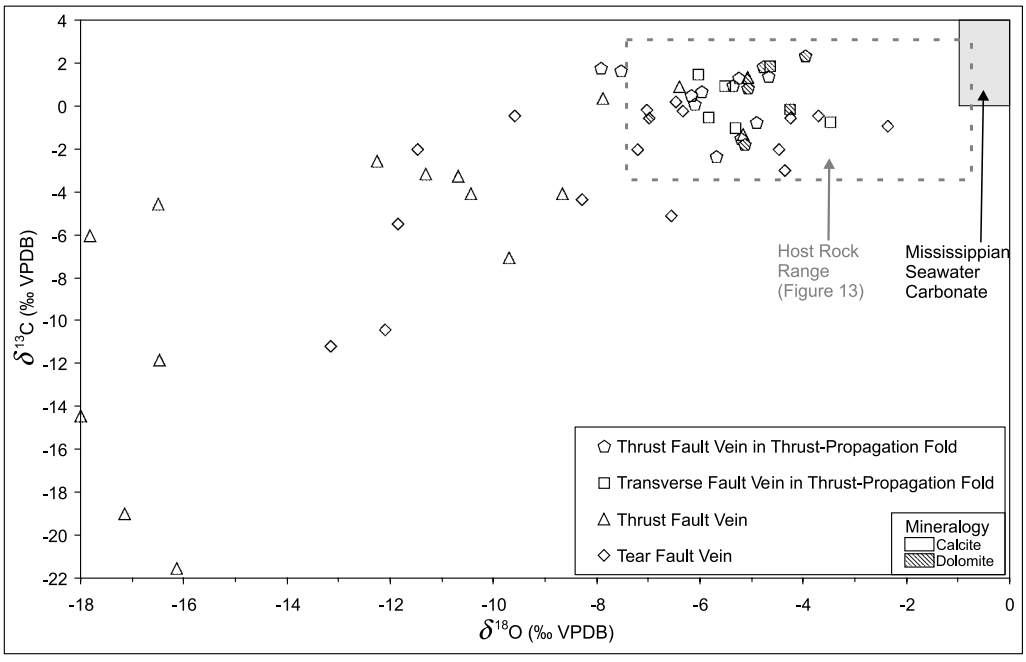


**Figure 14.** The $\delta^{18}O$ versus $\delta^{13}C$ values of carbonate veins collected from different types of structures in the Livingstone Range anticlinorium study area. Most of the veins associated with thrust-propagation folding have compositions that lie within the range of host rock compositions, represented by the box with the dashed outline. The shaded box represents proposed Mississippian seawater carbonate composition, where the $\delta^{18}O$ range is based on Killingly (1983) and Muehlenbachs (1998) and the $\delta^{13}C$ range is based on Veizer et al. (1999).

thrust faults, exhibit characteristics consistent with rocks that have been hydrothermally altered. They are lighter in color than the surrounding rocks; are weakly stained with iron oxides; and have sandy, granular textures in outcrop and milky, translucent to opaque textures in thin sections. Two of the altered host rocks are from the Turner Valley Member of the Livingstone Formation and have $\delta^{13}C$ values of +0.5 and –0.4‰, which are at least 1‰ lower than the $\delta^{13}C$ values of other samples of the Turner Valley Member (samples 209-R and 496-R in Table 1).

## Veins

Thrust-propagation folding in the LRA involved displacements along thrust faults and transverse faults within fold hinges and fold limbs. Veins from both of these fault zone types have $\delta^{18}O$ and $\delta^{13}C$ values that plot within a narrow range that overlaps the lower $\delta^{18}O$ range of most host rocks (Figure 14). Veins from thrust fault zones within thrust-propagation folds have $\delta^{18}O$ values that range from –7.9 to –4.0‰ and $\delta^{13}C$ values that range from –2.4 to +2.4‰ (Figure 14; Table 1). Vein samples collected from transverse faults that formed within fold limbs during thrust-propagation folding have $\delta^{18}O$ values that range from –6.0 to –3.5‰ and $\delta^{13}C$ values that range from –1.1 to +1.8‰ (Figure 14; Table 1).

Nineteen vein samples from major tear faults that cut across the LRA have $\delta^{18}O$ values that range from –13.1 to –2.4‰ and $\delta^{13}C$ values that range from –10.5 to –0.2‰. Ten of these veins have $\delta^{18}O$ and $\delta^{13}C$ values that are similar to those of host rock values (Figure 14).

Veins from major and minor thrust fault zones that are not related to thrust-propagation folding have the lowest $\delta^{18}O$ values that range from –18.0 to –4.4‰ and low $\delta^{13}C$ values that range from –21.6 to +1.3‰. However, three vein samples from thrust faults have $\delta^{18}O$ and $\delta^{13}C$ values that lie within the range of host rock isotopic compositions (Figure 14; Table 1).

### Stable Isotope Thermometry

Temperatures of vein formation were calculated for five samples from fault zones within the Centre Peak anticline that are interpreted to have been active during thrust-propagation folding (Table 2). Coexisting oxygen-bearing minerals within these veins are assumed to have precipitated in isotopic equilibrium with each other and coeval water. Calcite and dolomite in these veins have irregular

**Table 2.** Apparent Equilibration Temperatures and Coeval Water Compositions Calculated from $\delta^{18}O$ Values of Calcite, Dolomite ± Quartz in Veins in Fault Zones in the Centre Peak Anticline

| Vein Sample* | Structure | Calcite $\delta^{18}O$ (‰)** | Dolomite $\delta^{18}O$ (‰)** | Quartz $\delta^{18}O$ (‰)** | Water $\delta^{18}O$ (+1.7/–2.3‰)** | Temperature (±50°C) |
|---|---|---|---|---|---|---|
| 198B-V2 | Thrust fault in thrust-propagation fold | –6.2 | –5.0 | | –13.0 | 250 |
| | | –6.2 | –5.1 | | –12.6 | 260 |
| 198D-V2 | Thrust fault in thrust-propagation fold | –5.3 | | –3.0 | –12.1 | 250 |
| | | | –4.0 | –3.0 | –11.5† | 260 |
| | | –5.3 | –4.0 | | –12.9 | 230 |
| | | –5.2 | | –3.0 | –11.7 | 260 |
| | | –5.2 | –4.0 | | –11.9 | 250 |
| 190-V2 | Thrust fault in thrust-propagation fold | –6.0 | –4.8 | | –12.8 | 250 |
| 688A-V2 | Transverse fault in thrust-propagation fold | –5.8 | –4.6 | | –12.7 | 250 |
| 188A-V2 | Transverse fault in thrust-propagation fold | –5.3 | –4.3 | | –10.9 | 280 |
| | | –5.4 | –4.3 | | –11.9 | 260 |

*All sample locations are shown in Figure 3.
**All $\delta^{18}O$ values are reported relative to Vienna Peedee belemnite in units of per mil (‰).
†The error associated with the temperature calculation is approximately ±50°C, which represents a range in $\delta^{18}O$ values for coeval water of +1.7/–2.3‰ for calcite/water and +1.9/–2.5‰ for dolomite/water.

intergrowth textures that show no evidence of sequential growth; neither calcite nor dolomite preferentially grew along vein margins, and no vein centerlines consisting of only one mineral were present (Figure 12D). Quartz in veins at sample locality 198 (Figure 3) occurs as randomly oriented subhedral radiating crystal aggregates or euhedral doubly terminating single crystals that are in contact with either calcite or dolomite (Figure 12D). Mineral textures are consistent with these minerals precipitating together as a result of an abrupt pressure drop within dilatant fractures in faults that were active during folding.

In the hanging wall of the thrust fault that cuts along the hinge zone of the Centre Peak anticline at Green Creek, a set of east-west–trending, steeply dipping veins cut across the hinge zone of a tightly folded thrust duplex of lime mudstone and chert at the top of the Banff Formation (sample location 198, Figure 3; cross section AA′ in Figure 4). Oxygen isotopic compositions of calcite and dolomite from sample 198B-V2 provide apparent equilibrium temperatures near 250°C and an average $\delta^{18}O$ value of coeval water of –12.8‰ (Table 2). A second vein sample (198D-V2), which was collected less than 1 m (<3.3 ft) south of 198B-V2, has calcite, dolomite, and quartz with equilibration temperatures also averaging 250°C and an average $\delta^{18}O$ value for coeval water of –12.0‰ (Table 2).

Veins that are steeply dipping and north-south trending and that lie in the hanging wall of a thrust fault in the hinge zone of the Centre Peak anticline on the north side of Green Creek canyon (sample locality 190, Figure 3; cross section AA′ in Figure 4) contain calcite and dolomite that have an apparent equilibrium temperature of 250°C and a $\delta^{18}O$ value for coeval water of –12.8‰ (Table 2). Similarly, carbonate veins from a transverse fault zone that cuts the forelimb of the Centre Peak anticline, approximately 760 m (~2493 ft) south of Morin Creek (sample locality 688, Figure 3), contain calcite and dolomite that have an apparent equilibrium temperature of 250°C and a $\delta^{18}O$ value for coeval water of –12.7‰ (Table 2).

Carbonate veins within a transverse fault zone that cuts across the backlimb of the Centre Peak anticline occur approximately 600 m (~1969 ft) south of Morin Creek (sample locality 188, Figure 3). Calcite and dolomite from sample 188A-V2 provide apparent equilibrium temperatures of 280 and 260°C and an average $\delta^{18}O$ value for coeval water of –11.4‰ (Table 2).

The similarity of all these apparent equilibrium temperatures and inferred $\delta^{18}O$ values for

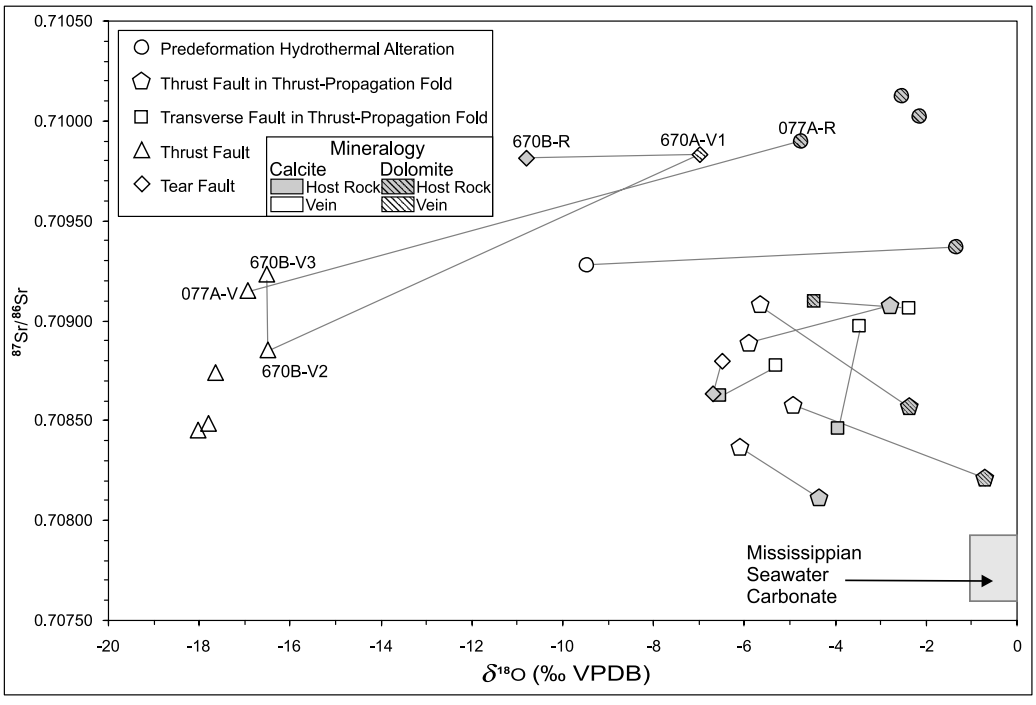


**Figure 15.** The $^{87}Sr/^{86}Sr$ ratios versus $\delta^{18}O$ values of veins and host rocks from the Livingstone Range anticlinorium. Hydrothermally altered host rocks (circles) have the highest $^{87}Sr/^{86}Sr$ ratios. Tie lines connect veins with their associated host rocks. The shaded box representing ideal Mississippian seawater carbonate composition is based on Killingly (1983) and Muehlenbachs (1998) for $\delta^{18}O$ and Veizer et al. (1999) for $^{87}Sr/^{86}Sr$. All veins and host rocks have high $^{87}Sr/^{86}Sr$ ratios relative to proposed Mississippian seawater carbonate values reported by Veizer et al. (1999).

coeval water (Table 2) implies that the thermal and fluid conditions were constant along the southern part of the Centre Peak anticline during the formation of these veins. The veins at sample locality 198 in particular are inferred to have formed during the later stages of thrust-propagation folding because they cut across the hinge zone of a tightly folded thrust duplex in the core of the Centre Peak anticline and are themselves only weakly deformed.

### Strontium Isotopic Ratios

Host rocks that are cut by prethrusting hydrothermal jasperoid chert veins are generally composed of dolomite with relatively high $^{87}Sr/^{86}Sr$ ratios ranging from 0.70937 to 0.71012 (Table 1; Figure 15). Host rocks from fault zones in thrust-propagation folds have lower $^{87}Sr/^{86}Sr$ ratios that range from 0.70812 to 0.70909 (Table 1; Figure 15). The $^{87}Sr/^{86}Sr$ ratios of all host rocks are higher than the expected range of 0.70767 to 0.70799 for Lower Mississippian seawater carbonate rocks (Veizer et al., 1999), indicating that they have been altered by fluids with high $^{87}Sr/^{86}Sr$ ratios.

The $\delta^{18}O$ values of most host rocks are similar, regardless of the type of fault in which they occur, except for one altered host rock (670B-R) from a tear fault zone cut by a thrust fault. This sample consists of recrystallized calcite with a very low $\delta^{18}O$ value of –10.8‰ and a high $^{87}Sr/^{86}Sr$ ratio of 0.70981 (Table 1; Figure 15).

Veins from fault zones in thrust-propagation folds have $^{87}Sr/^{86}Sr$ ratios that range from 0.70837 to 0.70908 (Table 1; Figure 15), similar to the range of 0.70812 to 0.70909 for $^{87}Sr/^{86}Sr$ ratios of the local host rocks. However, most individual veins in thrust-propagation folds have slightly higher $^{87}Sr/^{86}Sr$ ratios than the host rock with which they occur (Figure 15).

Calcite veins from thrust faults that are inferred to have been active during later stages of thrusting deformation have very low $\delta^{18}O$ values that range from –18.0 to –16.5‰. The $^{87}Sr/^{86}Sr$ ratios of these late calcite veins, which range from 0.70845 to 0.70923, are similar to the $^{87}Sr/^{86}Sr$ ratios of most host rocks.

The calcite veins that have the highest $^{87}Sr/^{86}Sr$ ratios and lowest $\delta^{18}O$ values are from young thrust faults that cut through host rocks with very high $^{87}Sr/^{86}Sr$ ratios (samples 670 and 070A, Figure 15), indicating that the $^{87}Sr/^{86}Sr$ ratios of veins are

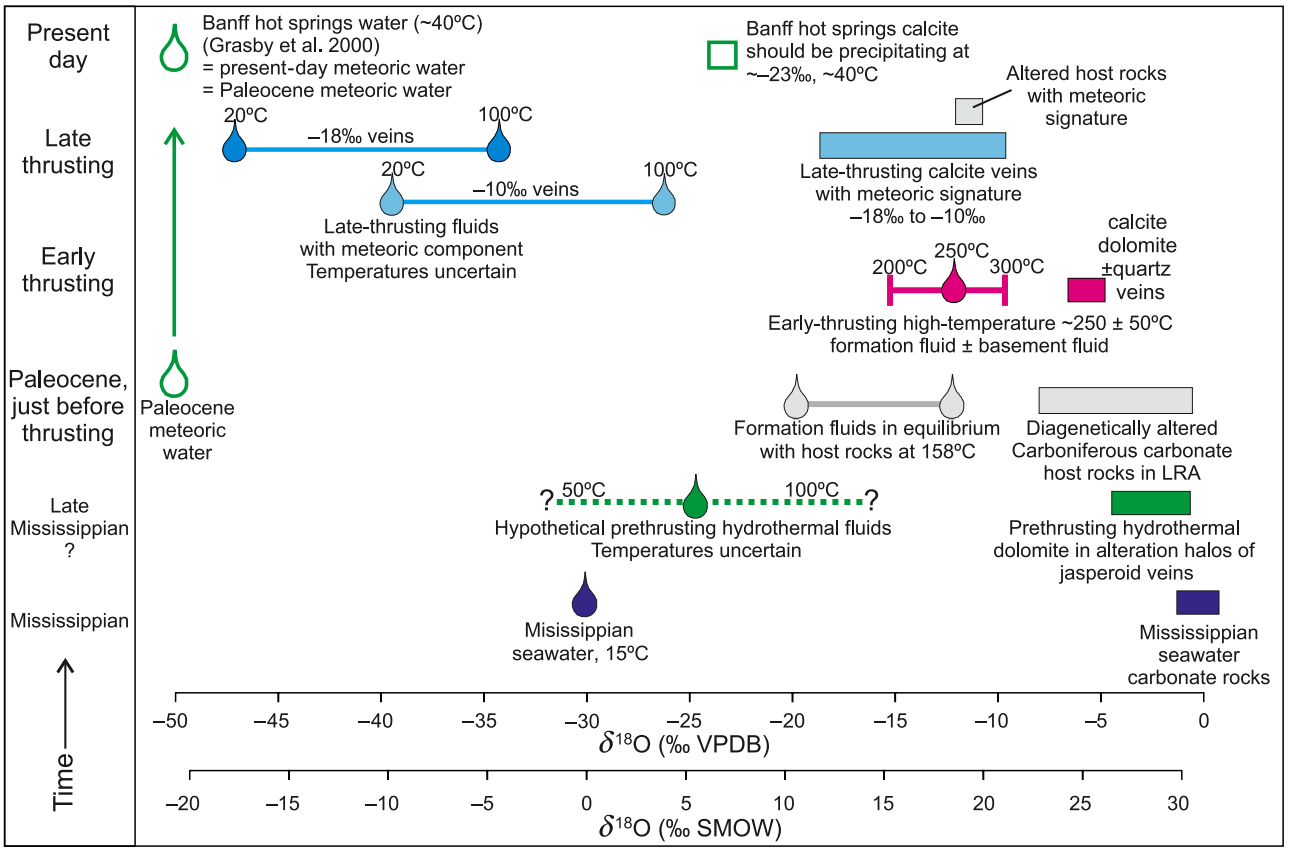


**Figure 16.** The thermal and fluid evolution in the Livingstone Range anticlinorium (LRA) deduced from $\delta^{18}O$ values of host rocks and veins.

strongly influenced by local host rock. Sample 670 is one location where an early vein with a high $\delta^{18}O$ value and a high $^{87}Sr/^{86}Sr$ ratio (Figure 15) is cut by a younger vein with a much lower $\delta^{18}O$ value and a lower $^{87}Sr/^{86}Sr$ ratio (sample 670B-V2, Figure 15).

The $^{87}Sr/^{86}Sr$ ratios for most veins lie within the range of the host rock, suggesting that the source of the strontium was the host rocks.

## INTERPRETATION

Isotopic compositions of host rocks and veins from different structures show distinct patterns that can be used to infer the types of fluids that were flowing through the structures at various tectonic stages. The $\delta^{18}O$ values are especially important for elucidating the thermal and fluid-flow history (Figure 16).

### Early Diagenesis and Hydrothermal Activity

The relatively low $\delta^{18}O$ values of both calcite and dolomite in host rocks in the LRA, relative to the expected value of approximately 0‰ (Killingly, 1983; Muehlenbachs, 1998), indicate that these rocks have been affected by diagenesis. In the Western Canada sedimentary basin, pervasive dolomitization affected much of the Paleozoic carbonate strata in several stages, beginning shortly after deposition and continuing after burial (Al-Aasm and Lu, 1994; Lewchuk et al., 1998; Cioppa et al., 2000). Diagenesis locally involved the systematic formation of new dolomite with successively lower $\delta^{18}O$ values with each diagenetic event, and it included the incorporation of variable amounts of radiogenic strontium (Al-Aasm and Lu, 1994; Lewchuk et al., 1998; Cioppa et al., 2000) with $^{87}Sr/^{86}Sr$ ratios that are higher than those expected from other Mississippian carbonates (Veizer et al., 1999). The

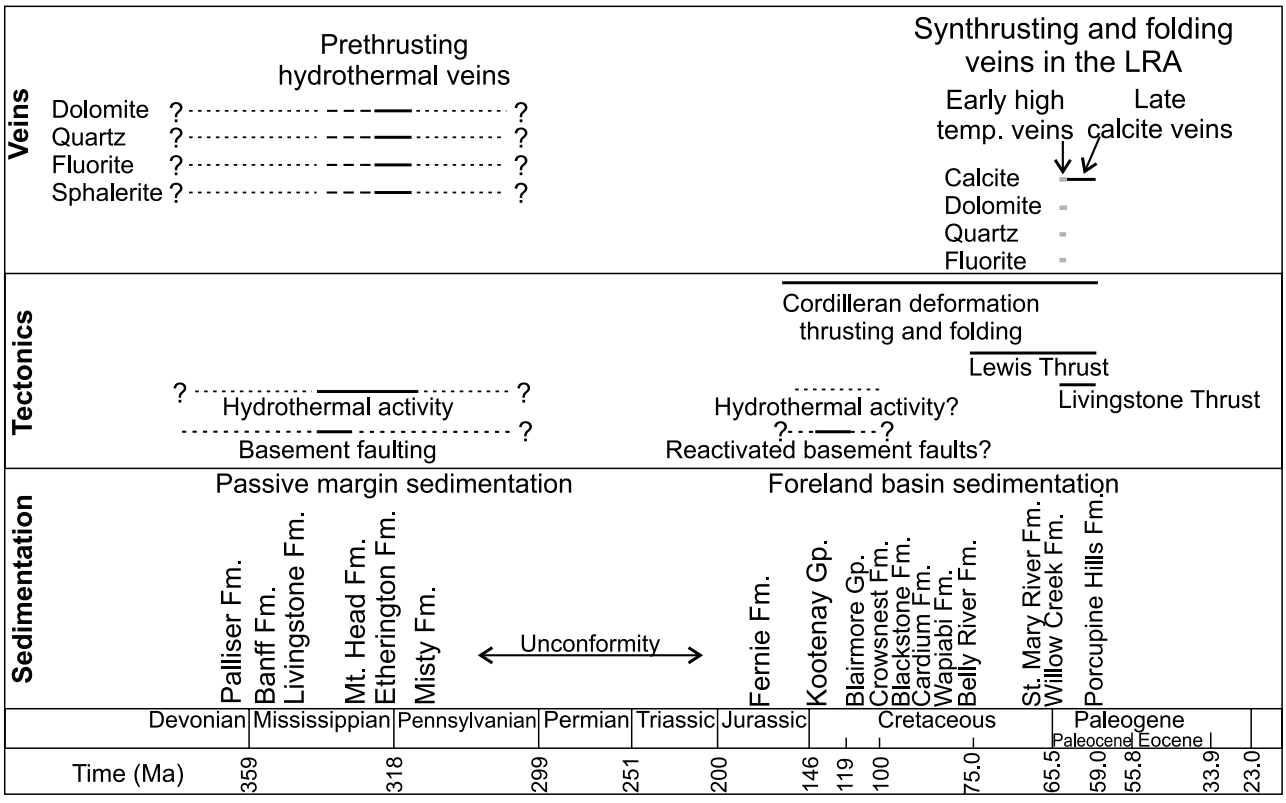


**Figure 17.** The paragenetic sequence of sedimentation, tectonic events, and fluid and/or veining events in the Livingstone Range anticlinorium (LRA).

$^{87}Sr/^{86}Sr$ ratios in host rocks in the LRA are similarly high, but the highest ratios are found in dolomitized host rock in alteration halos that surround prethrusting hydrothermal veins (Figure 15), indicating the presence of allochthonous fluids in the Mississippian rocks of the LRA. The temperatures at which these veins formed are unknown, but a hypothetical range of compositions and temperatures is depicted in Figure 16 for the predeformation hydrothermal fluids. The allochthonous fluids could have originated from the thick shale units of the underlying Banff and Exshaw formations, but a basement source for the fluids is supported in the LRA by the probable structural relationship between the east-southeast and north-northwest strikes of the horizontally restored bedding-perpendicular hydrothermal veins that are symmetrically distributed about the east-northeast–trending tear faults and transverse faults within the LRA. The Morin Creek tear fault (Figure 3), the Daisy Creek tear fault (Figure 5), and the smaller transverse faults in the limbs of the anticlines (Figure 10A) all terminate upward within the lower part of the Mount Head Formation, which indicates that these fractures formed in the Late Mississippian during deposition of the Mount Head Formation. Reactivation of basement faults during the Mississippian has been recognized regionally within the Mount Head Formation by abrupt changes in sedimentary facies and stratigraphic thickness across major basement structures (Brandley et al., 1996). The youngest strata found to contain prethrusting jasperoid veins are of the Upper Mississippian Etherington Formation, which suggests that possible reactivation of the faults and upward flow of basement fluids could have continued into the Pennsylvanian (Figure 17). Many of the veins in the Etherington Formation are parallel to bedding, suggesting that they formed at a time when the Etherington Formation was at a relatively shallow depth of burial.

The underlying Paleoproterozoic basement of western Canada and United States is composed of a collage of continental blocks separated by

ancient fault zones and sutures. The Vulcan structure of southern Alberta is one such structure (Figure 1). It is marked by a conspicuous east-northeast–trending regional negative bouguer gravity anomaly, and paired negative and positive aeromagnetic anomalies that are interpreted to mark an east-northeast–trending fault structure (Eaton et al., 1999; Clowes et al., 2002). Palinspastic restoration of the LRA approximately 40 km (~25 mi) westward to its approximate original prethrusting location aligns this part of the Livingstone Range above the southwest trend of the Vulcan Low. The east-northeast–trending transverse faults within the LRA may be related to fractures that were once controlled by the underlying Vulcan structure, which was probably active during the Late Mississippian, and may have been associated with upward migration of hydrothermal fluids with high $^{87}Sr/^{86}Sr$ ratios from the Paleoproterozoic crystalline basement before, during, and after diagenesis, providing the anomalously radiogenic strontium that was incorporated into the rocks during diagenesis.

An Early Cretaceous timing of basement fault reactivation and local hydrothermal activity is also possible (Figure 17). Early Cretaceous reactivation of basement structures, which has been attributed to thrust loading along the continental margin of western North America, has been documented elsewhere in the Canadian Cordillera (Hart and Plint, 1993; Lemieux, 1999).

## Early Synthrusting Formation Fluid Flow ± Basement Fluids

Thrust-propagation folds in the LRA are interpreted to have been more or less fully formed by the time the Livingstone thrust propagated up the ramp to the detachment in the Jurassic Fernie Formation. Most thrust-propagation folds in the LRA are chevron folds, a fold style that develops rapidly once initiated (Ramsay, 1974). The rapid dilation that accompanied folding caused fluids to be drawn into the dilatant zones in the folds during a relatively short-lived geologic event.

Vein samples collected from fault zones that are interpreted to have been active during thrust-propagation folding have $\delta^{18}O$ and $\delta^{13}C$ values that are similar to those of the local host rocks (Figure 14), which suggests that the veins formed from formation fluids that were in isotopic equilibrium with local lithology. The consistently lower $\delta^{13}C$ values of all veins relative to host rocks are interpreted to be caused by the addition of carbon from oxidized hydrocarbons, which is supported by the abundant occurrence of hydrocarbon fluid inclusions in the vein calcite and dolomite. A partial basement-derived source for these fluids is indicated by the generally higher $^{87}Sr/^{86}Sr$ ratios of most of these veins relative to their adjacent host rocks (Figure 15; Table 1) and by anomalously high temperatures of vein formation of approximately 250 ± 50°C calculated from oxygen-isotope thermometry of coexisting calcite and dolomite ± quartz from five veins near the top of the Banff Formation in the core of the Centre Peak anticline (Table 2). The paleotemperature for the top of the Banff Formation should have been approximately 158°C, assuming a depth of 5.5 km (3.4 mi), a geothermal gradient of 25°C/km, and an average surface temperature of 20°C.

The temperature of the top of the Banff Formation before thrusting and folding is related to the thickness of strata that lay above the Banff Formation before initial displacement along the Livingstone thrust. The Lewis thrust, the next major thrust to the west, has a maximum displacement of approximately 140 km (~87 mi) (Sears, 2001). It began moving at approximately 74 Ma and stopped at approximately 59 Ma (Sears, 2001; Osadetz et al., 2004). Assuming both the Lewis thrust and Livingstone thrust had similar displacement rates and both stopped moving at approximately 59 Ma, the Livingstone thrust, which has a displacement of approximately 40 km (~25 mi) in the Crowsnest Pass area, would have begun moving at approximately 64 Ma, during deposition of thick sand beds of the Paleocene Porcupine Hills Formation, which implies approximately 5.5 km (~3.4 mi) of strata lay above the Banff Formation just before the initial displacement on the Livingstone thrust.

The geothermal gradient of 25°C/km predicted for the LRA before thrusting deformation is based

on the assumption that geothermal gradient patterns have not changed significantly since the Paleocene. The present geothermal gradient in the undeformed sedimentary basin rocks of southwestern Alberta, just east of the thrust and fold belt, averages between 20 and 25°C/km (Bachu and Burwash, 1994). The prethrusting geothermal gradient that Osadetz et al. (2004) estimate for the Lewis thrust sheet before thrusting was 20°C/km.

The estimated paleotemperature of approximately 158°C for the top of the Banff Formation is in agreement with inferred temperatures calculated from vitrinite reflectance values of coal in the Jurassic–Cretaceous Kootenay Formation, which lies approximately 1 km above the top of the Banff Formation in the LRA. A vitrinite reflectance value of $R_o$ = 1.09% (Hacquebard and Donaldson, 1974) for the Kootenay Formation coal that lies to the west of the southern part of the Livingstone Range (Figure 3) gives a calculated temperature estimate of approximately 135°C using the method of Middleton (1982) or approximately 137°C using the method of Boyd and Lewis (1995). A temperature of approximately 133°C is obtained using a depth of approximately 4.5 km (~2.8 mi) for the Kootenay Formation coal, a geothermal gradient of 25°C/km, and a surface paleotemperature of 20°C.

The more than 40°C difference between the expected host rock temperature of approximately 158°C for the top of the Banff Formation and the vein precipitation temperatures of approximately 250 ± 50°C suggests that some of the fluid that formed these veins may have ascended from depths of more than 2 km below the top of the Banff Formation. The $\delta^{18}O$ values of the waters or fluids that formed these early synfolding veins ranged from –10.9 to –13.0‰ (Table 2; Figure 16). Host rocks at the expected temperature of approximately 158°C should have been in equilibrium with associated formation fluids with $\delta^{18}O$ values that ranged from –19 to –12‰ (Figure 16).

The isotopic compositions of veins that are related to thrust-propagation folding have a lower $\delta^{18}O$ limit of approximately –8.0‰ (Figure 14). This value is interpreted to represent the lowest probable isotopic composition for veins that formed from formation fluids and/or basement fluids. Veins with $\delta^{18}O$ values lower than –9‰ are interpreted to have formed from allochthonous fluids with anomalously low $\delta^{18}O$ values.

Many veins from tear faults and thrust faults that are not related to thrust-propagation folding also have $\delta^{18}O$ values that are similar to host rock compositions and $^{87}Sr/^{86}Sr$ ratios that are relatively high, which indicates that early movement along many of these faults also occurred when the structures were occupied by formation fluids and basement-derived fluids. In a few fault zones, earlier veins with $\delta^{18}O$ values that are similar to those of adjacent host rocks and younger veins with much lower $\delta^{18}O$ values are present (Table 1, sample locations 662, 670, and 671), indicating younger fault activity occurred when fluids with anomalously low $\delta^{18}O$ values were present.

Regional infiltration of basement-derived fluids from reactivated basement faults into thrust-related dilatant zones likely occurred along the entire thrust and fold belt as thrust faults were propagating eastward and incorporating new, previously undeformed strata. Machel and Cavell (1999) in their assessment of "squeegee" fluid flow suggested that relatively small amounts of basement fluids or fluids from Cambrian clastics entered the foreland basin in central Alberta during thrusting and folding deformation. Basement-derived fluids could have been infiltrating before and during all stages of thrusting and folding; however, during later thrusting-dominated stages, any isotopic evidence of basement fluids would have been diluted by the circulation of meteoric water.

## Late Synthrusting Meteoric Fluid Flow, Vein Formation, and Rapid Cooling

When the Livingstone thrust began propagating eastward along a detachment in the Fernie Formation, the LRA was transported eastward and elevating and exposed to erosion. Veins that formed along faults that were active during this later stage of thrust-dominated deformation have very low $\delta^{18}O$ values that range from approximately –9 to –18‰ (Figure 14) and are interpreted to have precipitated from variable amounts of meteoric water. The presence of oxidized hydrocarbons in

these veins is indicated by $\delta^{13}C$ values that are lower than –4‰, the lower $\delta^{13}C$ limit for host rocks (Figure 14). The Pocket Creek tear faults in particular contain veins with very low $\delta^{18}O$ values, supporting the structural interpretation that the Pocket Creek tear faults formed when the LRA became folded by the activity of younger underlying thrust faults.

Veins with similarly low $\delta^{18}O$ values have been documented in thrust faults in the Front Ranges of the southern Canadian Rocky Mountains near Banff (Figure 1) (Kirschner and Kennedy, 2001) and in subsurface thrust-related structures penetrated by petroleum exploration boreholes in the Foothills (Al-Aasm and Lu, 1994; Lewchuk et al., 1998; Cioppa et al., 2000). Thrust-transport deformation, which involved large displacements and included uplift and erosional exhumation, evidently coincided with deep penetration of meteoric fluids that left a regional isotopic record of tectonic veins in fault zones with low $\delta^{18}O$ values. This regional inundation of meteoric waters must have had a significant cooling thermal effect on the rocks through which they passed.

An investigation of the thermal history of the foreland thrust and fold belt in southern Alberta and British Columbia based on apatite fission-track thermochronology and vitrinite reflectance data has shown that rapid cooling of this part of the thrust belt coincided with displacement on the Lewis thrust (Figure 1) and other related faults (Osadetz et al., 2004). The geothermal gradient in the Lewis thrust sheet changed from approximately 20°C/km before thrusting to 8 to 12°C/km during thrusting. This change has been attributed to deep infiltration of cool meteoric water driven by high topography and facilitated by enhanced permeability because of brittle deformation (Osadetz et al., 2004).

The temperatures at which veins were forming at this time were likely quite variable, with locally low- or high-temperature zones being controlled by aperture widths of individual open fractures and the degree of connectivity of fracture networks. The thrust belt was a dynamic fluid-flow system in which fluid conduits probably changed abruptly through time; as deformation caused some faults or fracture networks to open, elsewhere it caused other faults to close and restrict fluid flow, likely accompanied by precipitation of vein-forming minerals that also sealed off conduits. The thermal and tectonic model presented in Figure 18 implies that the veins that precipitated during the thrust transport stage occurred at temperatures less than 100°C. If the temperatures of circulating meteoric fluids ranged between 20 and 100°C, the corresponding $\delta^{18}O$ values of the waters would have ranged between –40 and –25‰ (Figure 16).

Cool meteoric water that circulated through the strata in sufficient quantities to remove heat and decrease geothermal gradients must have flowed along conduits that should be visible today by some degree of hydrothermal alteration of adjacent host rock. Locally, however, the lack of alteration along thrust faults examined by Kirschner and Kennedy (2001) in the Front Ranges of the Rocky Mountains and the absence of low $\delta^{18}O$ values in veins that occur more than 1 m (>3.3 ft) away from thrust faults led them to infer that only small volumes of meteoric fluids had passed through the faults that they examined.

In the LRA, three host rocks have anomalously low $\delta^{18}O$ values and slightly lower $\delta^{13}C$ values relative to most host rocks (Table 1, samples 209-R, 670B-R, and 496-R; Figure 13). These host rocks are generally lighter in color than the surrounding rocks; they are variably stained with limonite; and they have sandy, granular textures and milky, translucent to opaque textures in thin sections that indicate that these rocks have been altered. Their very low $\delta^{18}O$ values (–10.8 to –12.2‰, Figure 13; Table 1) relative to all other host rocks analyzed in the LRA suggest that they were along major conduits for meteoric fluid circulation.

Hot springs that flow in the Rocky Mountains today are analogous to the type of deeply penetrating meteoric fluid-flow systems that once cooled the rock mass during thrusting and folding. The very low $\delta^{18}O$ values of these hot spring waters show that they are meteoric waters (Grasby et al., 2000). Water flowing from the hot springs in Banff, Alberta (Figure 1), is saturated with respect to carbonate, and it should be precipitating calcite with

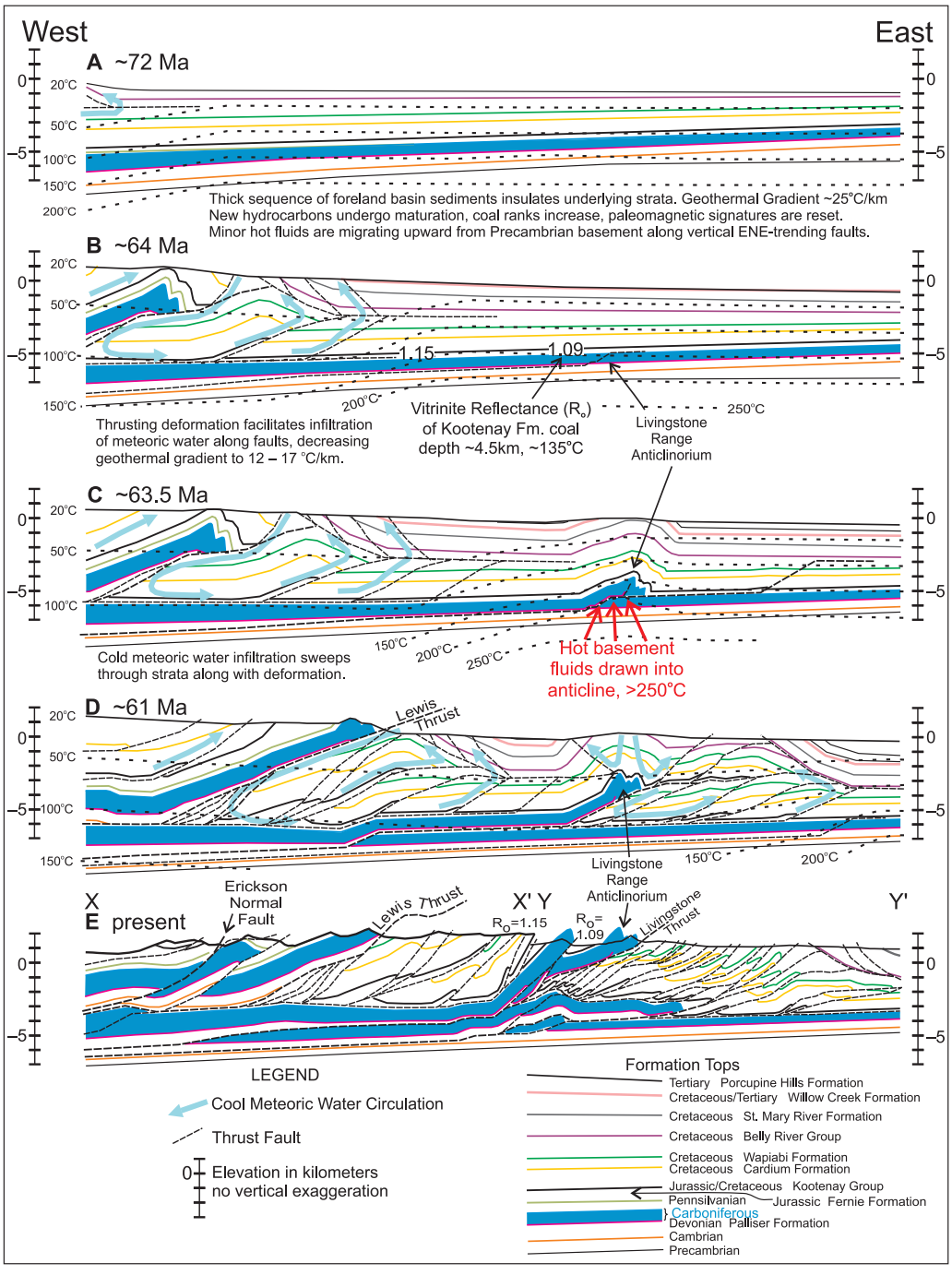


**Figure 18.** Hypothetical sequential palinspastic reconstruction of a composite balanced cross section showing the thermal, fluid, and deformation history of the southern Canadian Front Ranges and Foothills. Present-day cross sections XX′ and YY′ shown in panel E are modified from R. A. Price (2007, personal communication) and P. MacKay (2003, personal communication), respectively. Cross section locations are shown in Figure 1B. All ages are approximate and are based on the assumption that the initial movement of Livingstone thrust occurred at approximately 64 Ma (see text for discussion).

$\delta^{18}O$ values of approximately –24‰ (Figure 16) (calculated using data of Grasby et al., 2000). If veins were forming at depth along major conduits for meteoric fluid circulation during thrusting and folding, their isotopic compositions should be approximately –24‰. However, the lowest $\delta^{18}O$ values in calcite veins are –18‰ in the LRA, approximately –15‰ in the Front Range thrusts near Banff, Alberta (Kirschner and Kennedy, 2001), –17‰ in the subsurface Moose field (Cioppa et al., 2000), –12‰ in the subsurface Waterton gas field (Lewchuk et al., 1998), and –12‰ in the subsurface Quirk Creek field (Al-Aasm and Lu, 1994) (Figure 1). These $\delta^{18}O$ values are higher than approximately –24‰ and, therefore, likely represent meteoric fluids that had partly equilibrated with

host rocks before precipitating veins and, hence, were unlikely to have formed along the main conduits for meteoric fluid circulation. Evidence for significant meteoric fluid circulation perhaps should not be expected along the parts of thrust faults and tear faults that contain veins because veins are more likely to have formed where fluid flow became restricted or trapped in thin discontinuous fractures, allowing the meteoric fluids to be buffered by the host rocks and precipitate vein calcite.

Rapid cooling of the thrust and fold belt probably occurred by local circulation of significant volumes of meteoric fluid through relatively few major conduits. Cooling of the rest of the rocks mass was probably by conduction, analogous to the water-cooling system of the common internal combustion engine. Large volumes of meteoric fluids did not flush through the entire rock mass through every crack, fracture, and pore space. As thrusting deformation progressed from west to east, the region of circulating meteoric fluids and rapid cooling migrated along with the deformation (Figure 18A–D), flushing out the heat that had been contained by the thick insulating shale-bearing foreland basin deposits, abruptly and significantly lowering the regional geothermal gradient.

## DISCUSSION: THRUSTING CAUSES RAPID HEATING AND THEN RAPID COOLING OF THE FORELAND BASIN

The temperature increase that occurred in the foreland strata before thrusting and folding is interpreted by Bachu (1995) and Symons and Cioppa (2002) to result from sedimentary burial instead of from advective heating by displaced deep basin fluids, as predicted by Hitchon (1984). The temporary insulating effect of overlying foreland basin sediments that accumulated ahead of the deformation front resulted in increased maturation of coal and other hydrocarbons and caused the Late Cretaceous chemical remagnetization of the Paleozoic rocks (Enkin et al., 2000; Symons and Cioppa, 2002). The effects of this process on the rocks of the LRA are illustrated in Figure 18A, B. From Late Jurassic to Paleocene, more than 4.5 km (>2.8 mi) of strata accumulated in the foreland basin in the area that was eventually to become the LRA (Figure 18B). In the LRA, the foreland basin sediments likely continued to insulate the LRA during its earliest stage of thrust-propagation folding, temporarily allowing the Mississippian carbonate rocks to maintain the high temperatures of approximately 158°C proposed for the top of Banff Formation (Figure 18C). At the stage depicted in Figure 18C, the LRA had no through-going pathways for circulation of meteoric fluids, so no abrupt cooling would be expected at that time. However, once thrusting began to transport the LRA eastward, the formation of additional thrust faults and back thrusts allowed meteoric water to infiltrate the structure, abruptly cooling the LRA (Figure 18D).

The rapid cooling that occurs from circulating meteoric waters at the onset of thrusting deformation may explain the increase in vitrinite reflectance values of coal with depth in thrust repeats of Kootenay Formation coals intersected in many hydrocarbon exploration wells, as shown by Hacquebard and Cameron (1989). Although Hacquebard and Cameron (1989) attribute the increase of vitrinite reflectance with depth to be mainly caused by postdeformation coalification in the Kootenay Formation, they acknowledge that the same pattern is possible from the thrusting of coal with low rank over coal with a higher rank. The latter interpretation implies that as thrusting proceeded, coal-bearing strata that were insulated by relatively thin foreland basin deposits became faulted, folded, transported, elevated, and rapidly cooled by infiltrating meteoric water. Coal at the same stratigraphic level farther east in the as yet undeformed foreland basin would have been blanketed by thicker foreland basin deposits and would, therefore, have attained a higher rank than the coal that was about to be thrust over it. Continued repetition of this process would result in a structurally stacked series of coal horizons with systematically higher ranks with depth. This process has been proposed for the Grande Cache area of west-central Alberta (Figure 1) by Kalkreuth and McMechan (1984, 1996) to explain the high vitrinite reflectance values of coals that occur in

the Alberta syncline relative to successively lower ranks of equivalent coal strata that exist to the west and east.

## CONCLUSIONS

Basement faults have had an ongoing influence on the Western Canada sedimentary basin. Their intermittent activity has affected sedimentation, provided pathways for fluid migration, and influenced thrusting deformation. In the LRA, prethrusting and folding jasper ± fluorite ± sphalerite veins and adjacent dolomitic alteration halos with high $^{87}Sr/^{86}Sr$ ratios (0.7094–0.7101) and high $\delta^{18}O$ values (–4.8 to –1.3‰) relative to most host rocks (–7.92 to –1.08‰) may record the infiltration of Paleoproterozoic crystalline basement fluids into the Paleozoic strata along reactivated basement faults that were probably related to the underlying Vulcan structure. Basement-derived fluids may also have provided the radiogenic strontium that is recorded by the anomalously high $^{87}Sr/^{86}Sr$ ratios within diagenetically altered Paleozoic carbonate host rocks in the LRA and elsewhere in the Western Canada sedimentary basin. However, a shale basin source for the strontium is also very probable. Most tear faults that cut through the Livingstone thrust sheet and the transverse faults that preferentially cut the Livingstone Formation and older strata in the cores of the anticlines probably originated during Mississippian movement along underlying basement faults. These faults were subsequently reactivated during thrusting and folding.

Just before the formation of the LRA, the actively deforming parts of the thrust belt to the west were becoming thickened by thrust faults and elevated and exposed to erosion. As sediment was shed eastward from the emerging thrust belt, approximately 4.5 km (~2.8 mi) of strata accumulated in the foreland basin above the Paleozoic rocks that would eventually be incorporated into the LRA. The geothermal gradient was likely no greater than 25°C/km at this time, and the top of the Banff Formation, which was buried under approximately 5.5 km (~3.4 mi) of strata, achieved a maximum temperature of approximately 158°C, too hot for oil and gas preservation. Geothermal gradients in the undeformed eastern foreland basin abruptly increased during thrusting because of the rapid foreland basin sedimentation and not because of fluid flow, as Hitchon (1984) proposed.

During the earliest stages of thrusting deformation in the LRA, dilation that accompanied brittle chevron-style flexural-slip thrust-propagation folding caused formation fluids and small amounts of basement fluids to be drawn into the dilatant zones in the folds and into tear faults and larger thrust faults that were active at this time. These veins have $\delta^{18}O$ values that are similar to those of adjacent host rocks (–7.92 to –1.08‰), which support a formation fluid origin, but their slightly higher $^{87}Sr/^{86}Sr$ ratios indicate small amounts of fluids from the underlying crystalline basement. Most veins that precipitated at this time comprise both dolomite and calcite, and a few veins that formed near the top of the Banff Formation precipitated at anomalously high temperatures (250 ± 50°C) relative to the expected temperature of 158°C for this stratigraphic level, which also suggests a basement-derived fluid source.

Younger veins with low $\delta^{18}O$ values (–18 to –9‰) in thrust faults and tear faults are interpreted to have formed from a variable component of meteoric fluid that infiltrated during later stages of deformation while the LRA was being transported eastward and elevated by displacements on the Livingstone thrust and on underlying thrust faults. As thrusting deformation progressed from west to east, the region of infiltrating meteoric fluids and rapid cooling also migrated along with the deformation (Figure 18A–D), flushing out the heat that had been contained by the thick insulating layer of shale-bearing foreland basin deposits. The conduits along which significant meteoric fluid circulation occurred within the LRA are indicated in a few locations along faults where host rocks have been visibly strongly altered and have anomalously low $\delta^{18}O$ values (–10.8 to –12.2‰). The thrust belt was a dynamic fluid-flow system in which fluid conduits likely changed abruptly through time; whereas deformation caused some faults to open, elsewhere it caused other faults to close and restrict fluid flow, which may have been

accompanied by the precipitation of vein-forming minerals that sealed off conduits.

Significant hydrocarbon generation occurred during the relatively brief period of foreland basin sedimentation, forming hydrocarbon accumulations in sedimentary traps in the undeformed Jurassic to Eocene sediments. As thrusting deformation proceeded through the strata, potential structural hydrocarbon traps that developed could only have contained hydrocarbons if these traps formed either within or above strata that had been at hydrocarbon-favorable temperatures or if they were thrust above hydrocarbon source rocks that had been at favorable temperatures before thrusting. During the initial stages of thrust-propagation folding, the LRA would have been too hot for oil or gas preservation, and potential source rock strata that were downdip to the west would also have been overmature. Hydrocarbons could only have accumulated in the LRA during later stages of thrusting deformation when it became juxtaposed over Mesozoic source rocks in the footwall of the Livingstone thrust (Figure 18D).

Rapid cooling caused by infiltration of meteoric waters into the brittle crust of the deforming earth is likely not restricted to thrust and fold belts, nor is its thermal effect necessarily restricted to the upper few kilometers. The brittle crust above an active orogen is made deeply permeable during deformation, and deeply infiltrating meteoric waters will cool the rocks. Subsequent downward deflection of isotherms would effectively push down the brittle and/or ductile transition zone, enhancing even deeper meteoric fluid circulation that, in turn, would again push down the isotherms. This would form a metamorphic pattern of anomalously high pressures and/or low temperatures along the parts of an orogen that were the most permeable to meteoric fluid circulation, which may correspond to the parts of the orogen that were topographically highest.

## REFERENCES CITED


Al-Aasm, I. S., and F. Lu, 1994, Multistage dolomitization of the Mississippian Turner Valley Formation, Quirk Creek field, Alberta: Chemical and petrologic evidence: Canadian Society of Petroleum Geologists Memoir 17, p. 657–675.

Bachu, S., 1995, Synthesis and model of formation-water flow, Alberta Basin, Canada: AAPG Bulletin, v. 79, no. 8, p. 1159–1178.

Bachu, S., and R. A. Burwash, 1994, Geothermal regime in the Western Canada sedimentary basin, *in* G. D. Mossop and I. Shetsen, (comp.), Geological atlas of the Western Canada sedimentary basin: Canadian Society of Petroleum Geologists and Alberta Research Council Special Report 4: http://www.ags.gov.ab.ca/publications/wcsb_atlas/atlas.html (accessed October 4, 2010).

Boyd, R. J., and D. W. Lewis, 1995, Sandstone diagenesis related to varying burial depth and temperature in Greymouth coalfield, South Island, New Zealand: New Zealand Journal of Geology and Geophysics, v. 38, p. 333–348, doi:10.1080/00288306.1995.9514661.

Bradbury, J. H., and G. R. Woodwell, 1987, Ancient fluid flow within foreland terrains, *in* J. C. Goff and B. P. J. Williams, eds., Fluid flow in sedimentary basins and aquifers: Geological Society (London) Special Publicatrion 34, p. 87–02.

Brandley, R. T., F. F. Krause, J. L. Varsek, J. Thurston, and D. A. Spratt, 1996, Implied basement-tectonic control on deposition of Lower Carboniferous carbonate ramp, southern Cordillera, Canada: Geology, v. 24, no. 5, p. 467–470, doi:10.1130/0091-7613(1996)024<0467:IBTCOD>2.3.CO;2.

Burtner, R. L., and A. Nigrini, 1994, Thermochronology of the Idaho-Wyoming thrust belt during the Sevier orogeny: A new, calibrated, multiprocess thermal model: AAPG Bulletin, v. 78, no. 10, p. 1586–1612.

Cioppa, M. T., I. S. Al-Aasm, D. T. A. Symons, M. T. Lewchuk, and K. P. Gillen, 2000, Correlating paleomagnetic, geochemical and petrographic evidence to date diagenetic and fluid flow events in the Mississippian Turner Valley Formation, Moose field, Alberta, Canada: Sedimentary Geology, v. 131, no. 3–4, p. 109–129, doi:10.1016/S0037-0738(99)00134-7.

Clayton, R. N., and T. K. Mayeda, 1963, The use of pentafluoride in the extraction of oxygen from silicates and oxides for isotopic analysis: Geochimica et Cosmochimica Acta, v. 27, p. 43–52, doi:10.1016/0016-7037(63)90071-1.

Clayton, R. N., J. R. O'Neil, and T. K. Mayeda, 1972, Oxygen isotope exchange between quartz and water: Journal of Geophysical Research, v. 77, no. 17, p. 3057–3067.

Clowes, R. M., M. J. A. Burianyk, E. R. Kanasewich, and A. R. Gorman, 2002, Crustal velocity structure from SAREX, the Southern Alberta Refraction Experiment 1: Canadian Journal of Earth Sciences, v. 39, p. 351–373, doi:10.1139/e01-070.

Cooley, M. A., 2007, The structural, thermal, and fluid evolution of the Livingstone Range anticlinorium, and its regional significance to the southern Alberta foreland thrust and fold belt: Ph.D. thesis, Queen's University, Kingston, Ontario, Canada, 163 p.

Cooley, M. A., R. A. Price, J. M. Dixon, and T. K. Kyser, 2011, Along-strike variations and internal details of chevron-style, flexural-slip thrust-propagation folds

within the southern Livingstone Range anticlinorium, a paleohydrocarbon reservoir in southern Alberta Foothills, Canada: AAPG Bulletin, v. 95, no. 11, p. 1821–1849, doi:10.1306/01271107097.

Eaton, D. W., G. M. Ross, and R. M. Clowes, 1999, Seismic-reflection and potential-field studies of the Vulcan structure, western Canada: A Paleoproterozoic pyrenees?: Journal of Geophysical Research, v. 104, no. B10, p. 23,255–23,269, doi:10.1029/1999JB900204.

Enkin, R. J., K. G. Osadetz, J. Baker, and D. Kisilevsky, 2000, Orogenic remagnetizations in the front ranges and inner foothills of the southern Canadian Cordillera: Chemical harbinger and thermal handmaiden of Cordilleran deformation: Geological Society of America Bulletin, v. 112, p. 929–942, doi:10.1130/0016-7606(2000)112<929:ORITFR>2.0.CO;2.

Grasby, S. E., I. Hutcheon, and H. R. Krouse, 2000, The influence of water-rock interaction on the chemistry of thermal springs in western Canada: Applied Geochemistry, v. 15, p. 439–454, doi:10.1016/S0883-2927(99)00066-9.

Hacquebard, P. A., and A. R. Cameron, 1989, Distribution and coalification patterns in Canadian bituminous and anthracite coals: International Journal of Coal Geology, v. 13, no. 1–4, p. 207–260, doi:10.1016/0166-5162(89)90095-5.

Hacquebard, P. A., and J. R. Donaldson, 1974, Rank studies of coals in the Rocky Mountains and Inner Foothills Belt, Canada: Geological Society of America Special Paper 153, p. 75–94.

Hart, B. S., and A. G. Plint, 1993, Tectonic influence on deposition and erosion in a ramp setting: Upper Cretaceous Cardium Formation, Alberta foreland basin: AAPG Bulletin, v. 77, p. 2092–2107.

Hitchon, B., 1984, Geothermal gradients, hydrodynamics, and hydrocarbon occurrences, Alberta, Canada: AAPG Bulletin, v. 68, p. 713–743.

Holcombe, R. J., GEOrient© v9.x: http://www.holcombe.net.au/software/rodh_software_georient.htm (accessed May 1, 2011).

Kalkreuth, W., and M. E. McMechan, 1984, Regional pattern of thermal maturation as determined from coal rank-studies, Rocky Mountain Foothills and Front Ranges north of Grande Cache, Alberta: Implications for petroleum exploration: Bulletin of Canadian Petroleum Geology, v. 32, no. 3, p. 249–271.

Kalkreuth, W., and M. E. McMechan, 1996, Coal rank and burial history of Cretaceous–Tertiary strata in the Grande Cache and Hinton areas, Alberta, Canada: Implications for fossil fuel exploration: Canadian Journal of Earth Science, v. 33, p. 938–957, doi:10.1139/e96-071.

Killingly, J. S., 1983, Effects of diagenetic recrystallization on $^{18}O^{13}C$ values of deep-sea sediments: Nature, v. 301, p. 594–597, doi:10.1038/301594a0.

Kirschner, D. L., and L. A. Kennedy, 2001, Limited syntectonic fluid flow in carbonate-hosted thrust faults of the Front Ranges, Canadian Rockies, inferred from stable isotope data and structures: Journal of Geophysical Research, B, Solid Earth and Planets, v. 106, no. 5, p. 8827–8840, doi:10.1029/2000JB900414.

Lemieux, S., 1999, Seismic reflection expression and tectonic significance of Late Cretaceous extensional faulting of the Western Canada sedimentary basin in southern Alberta: Bulletin of Canadian Petroleum Geology, v. 47, no. 4, p. 375–390.

Lewchuk, M. T., I. S. Al-Aasm, D. T. A. Symons, and K. P. Gillen, 1998, Dolomitization of Mississippian carbonates in Shell Waterton gas field, southwestern Alberta: Insights from paleomagnetism, petrology and geochemistry: Bulletin of Canadian Petroleum Geology, v. 46, no. 3, p. 387–410.

Machel, H. G., and P. A. Cavell, 1999, Low-flux, tectonically induced squeegee fluid flow ("hot flash") into the Rocky Mountain foreland basin: Bulletin of Canadian Petroleum Geology, v. 47, no. 4, p. 510–533.

Matthews, A., and A. Katz, 1977, Oxygen isotope fractionation during dolomitization of calcium carbonate: Geochimica et Cosmochimica Acta, v. 41, p. 1431–1438, doi:10.1016/0016-7037(77)90249-6.

McCrea, J. M., 1950, On the isotopic chemistry of carbonates and a paleotemperature scale: Journal of Chemical Physics, v. 18, p. 849–857, doi:10.1063/1.1747785.

Middleton, M. F., 1982, Tectonic history from vitrinite reflectance: Geophysical Journal of the Royal Astronomical Society, v. 68, no. 1, p. 121–132.

Monger, J. W. H., and R. A. Price, 1979, Geodynamic evolution of the Canadian Cordillera; progress and problems: Canadian Journal of Earth Sciences, v. 16, no. 3, p. 771–791.

Muehlenbachs, K., 1998, The oxygen isotopic composition of the oceans, sediments and the sea floor: Chemical Geology, v. 145, p. 263–273, doi:10.1016/S0009-2541(97)00147-2.

Nesbitt, B. E., and K. Muehlenbachs, 1995, Geochemistry of syntectonic, crustal fluid regimes along the lithoprobe southern Canadian transect: Canadian Journal of Earth Sciences, v. 32, p. 1699–1719, doi:10.1139/e95-134.

O'Neil, J. R., R. N. Clayton, and T. K. Mayeda, 1969, Oxygen isotope fractionation in divalent metal carbonates: The Journal of Chemical Physics, v. 51, no. 12, p. 5547–5558, doi:10.1063/1.1671982.

Osadetz, K. G., B. P. Kohn, S. Feinstein, and R. A. Price, 2004, Foreland belt thermal history using apatite fission-track thermochronology: Implications for Lewis thrust and Flathead fault in the southern Canadian Cordilleran petroleum province, *in* R. Swennen, F. Roure, and J. W. Granath, eds., Deformation, fluid flow, and reservoir appraisal in foreland fold and thrust belts: AAPG Hedberg Series 1, p. 21–48.

Price, R. A., 1967, The tectonic significance of mesoscopic subfabrics in the southern Rocky Mountains of Alberta and British Columbia: Canadian Journal of Earth Sciences, v. 4, no. 1, p. 39–70, doi:10.1139/e67-003.

Price, R. A., 1981, The Cordilleran foreland thrust and fold belt in the southern Canadian Rocky Mountains, *in* K. R. McClay and N. J. Price, eds., Thrust and nappe tectonics: Geological Society (London) Special Publication 9, p. 427–448.

Price, R. A., 1994, Cordilleran tectonics and the evolution of

the Western Canada sedimentary basin, *in* G. D. Mossop and I. Shetsen, comp., Geological atlas of the Western Canada sedimentary basin: Canadian Society of Petroleum Geologists and Alberta Research Council Special Report 4: http://www.ags.gov.ab.ca/publications/wcsb_atlas/atlas.html (accessed October 4, 2010).

Ramsay, J. G., 1974, Development of chevron folds: Geological Society of America Bulletin, v. 85, no. 11, p. 1741–1754, doi:10.1130/0016-7606(1974)85<1741:DOCF>2.0.CO;2.

Sears, J. W., 2001, Emplacement and denudation history of the Lewis-Eldorado-Hoadley thrust slab in the northern Montana Cordillera, U.S.A.: Implications for steady-state orogenic processes: American Journal of Science, v. 301, p. 359–373, doi:10.2475/ajs.301.4-5.359.

Symons, D. T. A., and M. T. Cioppa, 2002, Conodont CAI and magnetic mineral unblocking temperatures: Implications for the Western Canada sedimentary basin: Physics and Chemistry of the Earth, v. 27, p. 1189–1193.

Veizer, J., et al., 1999, $^{87}Sr/^{86}Sr$, $\delta^{13}C$, and $\delta^{18}O$ evolution of Phanerozoic seawater: Chemical Geology, v. 161, p. 59–88, doi:10.1016/S0009-2541(99)00081-9.

Wheeler, J. O., and P. McFeely, 1991, Tectonic assemblage map of the Canadian Cordillera and adjacent parts of the United States of America: Geological Survey of Canada Map 1712A, scale 1:20,000,000.